Diffuse Domain Methods with Dirichlet Boundary Conditions

Luke Benfield*, Andreas Dedner

Mathematics Institute, University of Warwick, Coventry, CV4 7AL, UK

Abstract

The solution of partial differential equations (PDEs) on complex domains often presents a significant computational challenge by requiring the generation of fitted meshes. The Diffuse Domain Method (DDM) is an alternative which reformulates the problem on a larger, simple domain where the complex geometry is represented by a smooth phase-field function.

This paper introduces and analyses several new DDM methods for solving problems with Dirichlet boundary conditions. We derive two new methods from the mixed formulation of the governing equations. This approach transforms the essential Dirichlet conditions into natural boundary conditions. Additionally, we develop coercive formulations based on Nitsche's method, and provide proofs of coercivity for all new and key existing approximations.

Numerical experiments demonstrate the improved accuracy of the new methods, and reveal the balance between L^2 and H^1 errors. The practical effectiveness of this approach is demonstrated through the simulation of the incompressible Navier-Stokes equations on a benchmark fluid dynamics problems.

Keywords: Complex Domains, Diffuse Domain Methods, Smoothed Boundary Method, Partial Differential Equations, Signed Distance Functions

1. Introduction

Solving partial differential equations (PDEs) on domains with complex geometries is a significant challenge in computational science and engineering disciplines. Traditional numerical methods usually depend on generating a fitted mesh, which can be computationally expensive. Due to the boundary complexities, it is necessary to use a very fine mesh that is often smaller than the solution's length scale. This challenge is particularly present in three dimensions, and problems involving evolving boundaries. To overcome these difficulties of mesh generation, a variety of methods have been developed. For example, using a simple fitted mesh and modifying the discretization near the boundary, such as the Extended Finite Element Method [18]. On the other hand, there are methods that utilise non-fitted meshes, such as: the Fictitious Domain Method [20, 41, 51, 38], and the Immersed Boundary Method [32, 39, 21].

Among these approaches, the Diffuse Domain Method (DDM) has been created [30] as a particularly simple approach. The core concept is to embed the original, complex domain Ω into a larger, simple domain B. Therefore, it avoids the need for complex mesh generation, or explicit boundary tracking. The problem's geometry is represented by a phase field function, ϕ, which smoothly transitions between zero and one across a thin interfacial layer that approximates the boundary $\partial\Omega$. This transforms the problem of complex geometry into a problem of modifying the system's equations with terms dependent on ϕ. The main advantage of this method is its compatibility with standard finite element solvers, as it doesn't require unique additional terms.

*Corresponding author

Email addresses: luke.benfield@warwick.ac.uk (Luke Benfield), a.s.dedner@warwick.ac.uk (Andreas Dedner)

It is important to acknowledge that the Diffuse Domain method is a collection of different approximations which follow the above concept. Asymptotic analysis has been shown for several approximations for Dirichlet, Neumann, and Robin boundary conditions, [33, 52, 31, 37]. These methods have been developed to work on surface domains [43], and coupled bulk-surface systems [49, 1]. Also, there are similar approaches such as the Smoothed Boundary method [53, 54, 50].

The method has been successfully applied to a wide range of problems, from biology [2, 37, 36, 14] to materials [13, 42, 10]. Our experiment goal will be to apply this to the Navier-Stokes equations [3, 24, 5, 50]. This problem is a mixed system, however there haven't been explorations into developing a Diffuse Domain method from the mixed form of a PDE.

Typically, Diffuse Domain method formulations are derived by modifying the strong form or the weak form of the PDE with multiplying by ϕ and including an additional boundary term. This paper explores the development of new DDM formulations derived from combining these together with the mixed formulation of the equations. Hence, the Dirichlet boundary become natural boundary conditions within the formulation, which can lead to improved accuracy of the solution gradient. This type of boundary conditions are most commonly used in the benchmark experiments. Furthermore, we follow the approach of Nitsche's method, another well-established technique for the weak enforcement of boundary conditions [17] and has previously been used with the Diffuse Domain method [37, 35]. Along with the derivation of these new methods, we will show proof of coercivity, including the standard Diffuse Domain methods.

The paper is organised as follows. Section 2 introduces the key concepts of the Diffuse Domain method and the basic approximation methods. Section 3 derives the Nitsche's based Diffuse Domain approaches. In Section 4, we introduce the new methods based on the mixed formulation. Section 5 addresses the specific challenges and stabilisation terms for advection-dominated problems. Section 6 presents a set of numerical results focusing on application to advection-diffusion equations with Dirichlet boundary conditions, and resulting in benchmark problems of the incompressible Navier-Stokes equations to validate and compare the methods.

2. Diffuse Domain Method

2.1. Background

Starting with the example of Poisson's equation in a complex domain, Ω, with Dirichlet boundary conditions:

$$-\nabla \cdot (D\nabla u) = f \quad \text{in } \Omega, \tag{1a}$$
$$u = g \quad \text{on } \partial\Omega, \tag{1b}$$

where $D := D(x) \geq d > 0$ is a scalar function. To convert this problem into the Diffuse Domain framework on the extended domain, $B \supset \Omega$, we need to construct a phase-field function ϕ satisfying

$$\phi(x) \approx \chi_\Omega = \begin{cases} 1 & x \in \Omega; \\ 0 & x \in B \setminus \Omega. \end{cases} \tag{2}$$

Definition 1. We will use the following common approximation [33],

$$\phi(x) = \frac{1}{2}\left(1 - \tanh\left(\frac{3r(x)}{\epsilon}\right)\right), \; x \in B. \tag{3}$$

Here $r(x)$ is the signed distance function for the original domain; giving a negative distance from x to $\partial\Omega$ when $x \in \Omega$, and a positive distance from x to $\partial\Omega$ when $x \in B \setminus \Omega$. Note, ϵ is a small parameter to determine the width of the smooth interfacial region. The above ϕ gives an interface width of approximately 2ϵ.

Lemma 1. *It is simple to show that the gradient of this phase-field is*

$$\nabla\phi = -\frac{6}{\epsilon}\phi(x)(1 - \phi(x))\nabla r(x). \tag{4}$$

For later proofs, it is useful to define the separate regions where the behaviour of ϕ changes.

Definition 2. Define separate domains for the interior, exterior, and interface in terms of ϕ

$$B_{\text{int}} = \{x : \phi(x) = 1\}, \tag{5a}$$
$$B_{\text{ext}} = \{x : \phi(x) = 0\}, \tag{5b}$$
$$B_{\Gamma} = \{x : 0 < \phi(x) < 1\}. \tag{5c}$$

Focusing on methods explored in [33, 52], these suggest two core ideas for constructing approximations for the Poisson problem with $D = 1$ and Dirichlet boundary conditions.

$$\text{DDM1}: \quad -\nabla \cdot (\phi \nabla u) + \epsilon^{-3}(1-\phi)(u-\overline{g}) = \phi\overline{f}, \tag{6a}$$
$$\text{DDM2}: \quad -\phi\Delta u + \epsilon^{-2}(1-\phi)(u-\overline{g}) = \phi\overline{f}. \tag{6b}$$

This requires defining extensions $\overline{f}$ and $\overline{g}$ of f and g, respectively. We smoothly extend both function so that they are constant in the normal direction to the original boundary, $\partial\Omega$ extending g both into Ω and Ω^c and f only into Ω^c.

To compute this extension we will need to use the surface delta, $\delta_{\partial\Omega}$, such that

$$\int_B h\delta_{\partial\Omega}\, dx = \int_{\partial\Omega} h\, dS, \tag{7}$$

for all smooth function h. Following [33], a common approximation of the surface delta is

$$\delta_{\partial\Omega} \approx |\nabla\phi|. \tag{8}$$

Note, this has the property, $\nabla\phi = -\delta_{\partial\Omega} n$. So we approximate the outward unit normal of $\partial\Omega$ as,

$$\overline{n}(x) = -\frac{\nabla\phi(x)}{|\nabla\phi(x)|}. \tag{9}$$

Therefore, for the normal direction extensions we use

$$x = X(s) + r(x)n(s) \quad \forall x \in B, \tag{10}$$

where $X(s)$ is a parametric equation representation of the boundary $\partial\Omega$, $\mathrm{n}(s)$ is the unit outward normal, and s be the arclength.

Definition 3. We define the extensions for the forcing f and boundary data g using

$$\overline{g} = g(x + r(x)\overline{n}(x)), \tag{11}$$

and

$$\overline{f} = \begin{cases} f(x) & x \in \Omega, \\ f\left(x + r(x)\overline{n}(x)\right) & x \in B\backslash\Omega. \end{cases} \tag{12}$$

For simplicity, we will denote both the original functions and the extensions by f and g.

This extension is only required in a small neighbourhood around the boundary. For example, f is defined in Ω, and is only included when $\phi > 0$. In [33], their analysis states the neighbourhood $x \in B : |r(x)| << 1$, and [52] states this extension must be a minimum range of 3ϵ.

2.2. Weak Form Derivation

First we will look at the derivation of DDM1 (6a), which involves transforming the weak form. The model Poisson problem will become: Find $u \in H_0^1(\Omega) + g$

$$\int_\Omega D\nabla u \cdot \nabla v \, dx = \int_\Omega fv \, dx, \quad \forall v \in H_0^1(\Omega). \tag{13}$$

Introducing the phase field function to extend the domain into B gives: Find $u \in H_0^1(B) + g$

$$\int_B \phi D\nabla u \cdot \nabla v \, dx + \int_B B.C. \; v \, dx = \int_B \phi f v \, dx, \quad \forall v \in H_0^1(B), \tag{14}$$

where $B.C.$ is an additional term to incorporate the boundary conditions, and defines what PDE is solved in the external domain. Using integration by parts with the fact ϕ and v vanishes on the boundary of ∂B, we see that

$$\int_B -\nabla \cdot (\phi D \nabla u) \, v \, dx + \int_B B.C. \; v \, dx = \int_B \phi f v \, dx. \tag{15}$$

Many alternatives exist for $B.C.$ however, following DDM1, we take

$$B.C. \propto (1-\phi)(u-g). \tag{16}$$

The asymptotic analysis provided [33] suggests a scaling of ϵ^{-3} should be chosen. This is supported by the results from [16], where the scaling factor of ϵ^{-a} is used and demonstrates $\alpha \geq 2$ is necessary. Experimental results show a benefit of scaling this in proportion to the diffusion. Writing this method in the bilinear form gives the first method,

Method 1 (DDM1). Find $u \in U$ such that

$$a(u,v) := \int_B \phi D\nabla u \cdot \nabla v + \frac{D}{\epsilon^3}(1-\phi)uv \, dx, \tag{17}$$

$$l(v) := \int_B \phi f v + \frac{D}{\epsilon^3}(1-\phi)gv \, dx. \tag{18}$$

For all $v \in V$, where $V = H_0^1(B)$ and $U = V + g$.

We can now explore some important properties of this method.

Theorem 2. *DDM1 (Method 1) is symmetric and coercive i.e.,*

$$a(u,v) \geq c\|u\|^2$$

for a constant $c > 0$, with the norm

$$\|u\|^2 := \int_B \phi|\nabla u|^2 + \epsilon^{-3}(1-\phi)u^2 \, dx \tag{19}$$

on $H_0^1(B)$.

Proof. We can clearly see that the bilinear form is symmetric with $a(u,v) = a(v,u)$. Furthermore, it is straightforward to see coercivity.

$$\int_B \phi|\nabla u|^2 + \epsilon^{-3}(1-\phi)u^2 \, dx \geq \int_B \phi|\nabla u|^2 \, dx + \epsilon^{-3}\int_B (1-\phi)u^2 \, dx, \tag{20}$$

$$= C\|u\|^2. \tag{21}$$

It remains to show that $\|u\|$ is a norm on $H^1(B)$: we start by splitting the domain into three regions using Lemma 2. This gives,

$$\|u\|^2 = \int_{B_{\text{int}}} |\nabla u|^2 \, dx + \int_{B_\Gamma} \phi|\nabla u|^2 + \epsilon^{-3}(1-\phi)|u|^2 \, dx + \int_{B_{\text{ext}}} \epsilon^{-3}|u|^2 \, dx =: I_1 + I_\epsilon + I_0 \ . \tag{22}$$

Since each of the three terms is non-negative, $\|u\|^2 = 0$ implies

$$I_1 = 0 \implies u \text{ is constant in } B_{\text{int}}, \tag{23}$$

$$I_0 = 0 \implies u = 0 \text{ in } B_{\text{ext}}, \tag{24}$$

$$I_\epsilon = 0 \implies \phi|\nabla u|^2 + \epsilon^{-3}(1-\phi)|u|^2 = 0 \text{ in } B_\Gamma. \tag{25}$$

Again this implies each term in I_ϵ must be zero,

$$|\nabla u|^2 = |u|^2 = 0. \tag{26}$$

This can only hold true if $u = 0$ within the interfacial region. Due to the smoothness of u and the constant value in B_{int}, u must be equivalent to the interfacial region. Therefore, $u = 0$ everywhere. It is trivial to show the remaining properties to be a norm, from the similarity of this norm (19) to $\|\cdot\|_{H_0^1}$,

Note, this modification to the norm can be seen as a weighted norm, with ϕ defined as a positive function of the distance function [12]. □

2.3. Strong Form Derivation

For the derivation of DDM2, we first start with the strong form of the problem (1) and multiply by ϕ to obtain

$$-\phi\nabla\cdot(D\nabla u) = \phi f. \tag{27}$$

Applying the same extension into the extended domain, the weak form becomes

$$\int_B D\nabla u \cdot \nabla(\phi v) \, dx + \int_B B.C. \; v \, dx = \int_B \phi f v \, dx. \tag{28}$$

We will use the same $B.C.$ as DDM1 (16), however this time based on the same asymptotic analysis we use ϵ^{-2}. Thus, the weak form is,

Method 2 (DDM2). Find $u \in U$ such that

$$a(u,v) := \int_B D\nabla u \cdot \nabla(\phi v) + \frac{D}{\epsilon^2}(1-\phi)uv \, dx, \tag{29}$$

$$l(v) := \int_B \phi f v + \frac{D}{\epsilon^2}(1-\phi)gv \, dx. \tag{30}$$

For all $v \in V$, where $V = H_0^1(B)$ and $U = V + g$.

Exploring the same properties, we can clearly see the bilinear form is not symmetric. However, we are unable to comment about coercivity of this method but in section 3 we will derive a new method that is coercive.

Another approach to obtain a strong form equation on the extended domain is the Smoothed Boundary Method (SBM), a general framework is provided in [53].

We will explore the similarities of SBM derivation to the Diffuse Domain method by applying this to our example problem. First multiply equation (1) by ϕ and using the product rule we get,

$$-\nabla\cdot(\phi D\nabla u) + \nabla\phi\cdot(D\nabla u) = \phi f. \tag{31}$$

Repeating that step, results in

$$-\phi\nabla\cdot(\phi D\nabla u)+D\left[\nabla\phi\cdot\nabla(\phi u)-u|\nabla\phi|^2\right]=\phi f. \tag{32}$$

Recall, we approximate the surface delta with $\delta_{\partial\Omega}=|\nabla\phi|$. Therefore, we can use the Dirichlet boundary conditions $u=g$ in that term to give

$$-\phi\nabla\cdot(\phi D\nabla u)+D\nabla\phi\cdot\nabla(\phi u)-D|\nabla\phi|^2 g=\phi^2 f. \tag{33}$$

Typically, SBM and Diffuse Domain methods require a small offset to ϕ from 0 to make sure the problem is defined, and solvable on the exterior domain. To further explicitly define the external problems, we can add the same $B.C.$ term (16) from DDM1/DDM2 to all methods used.

While rigorous asymptotic analysis for this modification is a topic for future work, numerical experiments shows this maintains the accuracy of the method. Also, the experiments show that a scaling of ϵ^{-2} remains stable and provides the best accuracy. Therefore, this gives the following weak form:

Method 3 (SBM). Find $u\in U$ such that

$$a(u,v):=\int_B \phi D\nabla u\cdot\nabla(\phi v)+D\nabla\phi\cdot\nabla(\phi u)v+\frac{D}{\epsilon^2}(1-\phi)uv\;dx, \tag{34}$$

$$l(v):=\int_B \phi^2 fv+D|\nabla\phi|^2 gv+\frac{D}{\epsilon^2}(1-\phi)gv\;dx. \tag{35}$$

For all $v\in V$, where $V=H_0^1(B)$ and $U=V+g$.

Theorem 3. *SBM (Method 3) is coercive but not symmetric, with the norm*

$$\|u\|^2:=\int_B \phi|\nabla u|^2+\epsilon^{-2}(1-\phi)u^2\;dx. \tag{36}$$

Proof. The first two terms of the bilinear form clearly show it is not symmetric.

To show this is coercive, we can simply see that when $v=u$ the bilinear is

$$a(u,u)=\int_B \phi D\nabla u\cdot\nabla(\phi u)+D\nabla\phi\cdot\nabla(\phi u)u+\frac{D}{\epsilon^2}(1-\phi)|u|^2\;dx \tag{37}$$

$$=\int_B D|\nabla(\phi u)|^2+\frac{D}{\epsilon^2}(1-\phi)|u|^2\;dx. \tag{38}$$

This is identical, up to epsilon scalling, to DDM1, so following the results (Theorem 2), this method is coercive. □

3. Diffuse Domain Nitsche's Method

Nitsche's method is a classic method of weakly enforcing a Dirichlet boundary condition on a PDE [11, 28]. A general framework is presented in [8], including for the Poisson model equation (1). This approach adds a penalty term instead of enforcing the boundary condition directly in the function space. Therefore, allowing us to apply integration by parts, while keeping the consistency term to obtain:

$$\int_\Omega D\nabla u\cdot\nabla v\;dx-\int_{\partial\Omega} D\nabla u\cdot nv\;dS+\beta\int_{\partial\Omega}(u-g)v\;dS=\int_\Omega fv\;dx. \tag{39}$$

Note that, to make this method symmetric we can add this optional term

$$-\int_{\partial\Omega} D\nabla v\cdot n(u-g)\;dS. \tag{40}$$

This is summarised as,

$$\int_\Omega D\nabla u \cdot \nabla v \; dx - \int_{\partial\Omega} D\nabla u \cdot nv \; dS - \alpha \int_{\partial\Omega} D\nabla v \cdot n(u-g) \; dS + \beta \int_{\partial\Omega} (u-g)v \; dS = \int_\Omega fv \; dx. \tag{41}$$

The parameter $\alpha \in \{1, 0, -1\}$, controls if we have a symmetric, non-symmetric, or skew-symmetric form; β is the penalty factor for the boundary condition.

Thus, we apply the Diffuse Domain method using the first approach given in section 2.2, with the normal given by equation (9) and surface delta given as equation (8). To achieve the following,

$$\int_B \phi D\nabla u \cdot \nabla v + D\nabla u \cdot \nabla\phi v + \alpha D(u-g)\nabla\phi \cdot \nabla v + \beta(u-g)v|\nabla\phi| + B.C. \; v \; dx = \int_B \phi fv \; dx. \tag{42}$$

Remark 1. When we take $\alpha = \beta = 0$, Nitsche's method matches DDM2, so this method can be derived via section 2.3 as well. For Nitsche's method to be coercive, we require $\beta > 0$ in the case $\alpha \geq 0$. This suggests we can create a coercive DDM2 style method by adding these stabilising terms from Nitsche's methods in the Diffuse Domain framework.

From numerical experiments, using the same $B.C.$ from DDM2 (Method 2) preforms best. Therefore, by combining the first two terms, we use this weak form

$$\int_B D\nabla u \cdot \nabla(\phi v) + \frac{D}{\epsilon^2}(1-\phi)uv + \alpha D(u-g)\nabla\phi \cdot \nabla v + \beta(u-g)v|\nabla\phi| \; dx = \int_B \phi fv \; dx. \tag{43}$$

We will focus on the following two methods: a stabilised method with $\alpha = 0$, $\beta = \frac{3D}{2\epsilon}(1-\phi)$; and a stabilised symmetric method with $\alpha = 1$, $\beta = \frac{6D}{\epsilon}(1-\phi)$.

Method 4 (NDDM). Find $u \in U$ such that

$$a(u,v) := \int_B D\nabla u \cdot \nabla(\phi v) + \frac{D}{\epsilon^2}(1-\phi)uv + \frac{3D}{2\epsilon}(1-\phi)|\nabla\phi|uv \; dx, \tag{44}$$

$$l(v) := \int_B \phi fv + \frac{D}{\epsilon^2}(1-\phi)gv + \frac{3D}{2\epsilon}(1-\phi)|\nabla\phi|gv \; dx. \tag{45}$$

For all $v \in V$, where $V = H_0^1(B)$ and $U = V + g$.

Method 5 (NSDDM). Find $u \in U$ such that

$$a(u,v) := \int_B D\nabla u \cdot \nabla(\phi v) + \frac{D}{\epsilon^2}(1-\phi)uv + Du\nabla\phi \cdot \nabla v + \frac{6D}{\epsilon}(1-\phi)|\nabla\phi|uv \; dx \tag{46}$$

$$l(v) := \int_B \phi fv + \frac{D}{\epsilon^2}(1-\phi)gv + Dg\nabla\phi \cdot \nabla v + \frac{6D}{\epsilon}(1-\phi)|\nabla\phi|gv \; dx. \tag{47}$$

For all $v \in V$, where $V = H_0^1(B)$ and $U = V + g$.

Theorem 4. *NDDM (Method 4) and NSDDM (Method 5) are positive definite.*

Proof. Following the idea from DDM1 (Theorem 2) of splitting the domain into interface regions equation (5), we get the following bilinear form for $v = u$:

$$\int_{B_{\text{int}}} D|\nabla u|^2 \; dx + \int_{B_{\text{ext}}} \frac{D}{\epsilon^2}|u|^2 \; dx + \int_{B_\Gamma} D\phi|\nabla u|^2 + \frac{D}{\epsilon^2}(1-\phi)|u|^2 + D(\alpha+1)u\nabla u \cdot \nabla\phi + \frac{3D(\alpha+1)^2}{2\epsilon}(1-\phi)|\nabla\phi||u|^2 \; dx. \tag{48}$$

Therefore, we use the norm for $H_0^1(B)$ as

$$\|u\|^2 := \int_{B_{\text{int}}} |\nabla u|^2 \, dx + \int_{B_{\text{ext}}} \epsilon^{-2}|u|^2 \, dx + \int_{B_\Gamma} \epsilon^{-2}(1-\phi)|u|^2 \, dx, \tag{49}$$

Immediately following the previous proofs, we can see this is a norm in the regions B_{int}, B_{ext}. When $\|u\| = 0$ the interior, B_{int}, gives that u must be constant. Also, for the interface, B_Γ, and exterior, B_{ext}, gives that $u = 0$. Therefore, the constant value of u in B_{int} must match $u = 0$. Showing this is a norm because we have $u = 0$ everywhere.

Therefore, we are required to show B_Γ coincides with this norm. It is clear all terms in this integral are non-negative besides $u\nabla u \cdot \nabla\phi$, so that will be our focus. Recalling the gradient from Theorem 1, and since r is a signed distance function so $|\nabla r| = 1$; we replace a $\sqrt{|\nabla\phi|}$ to get the following.

$$\int_{B_\Gamma} D(\alpha+1)u\nabla u \cdot \nabla\phi \, dx \geq -\int_{B_\Gamma} D(\alpha+1)|u||\nabla u||\nabla\phi| \, dx \tag{50}$$

$$\geq -\int_{B_\Gamma} D(\alpha+1)|u||\nabla u|\sqrt{|\nabla\phi|}\sqrt{\frac{6}{\epsilon}(1-\phi)\phi} \, dx. \tag{51}$$

Using Young's Inequality this becomes,

$$-\int_{B_\Gamma} D(\alpha+1)|u||\nabla u|\sqrt{|\nabla\phi|}\sqrt{\frac{6}{\epsilon}(1-\phi)\phi} \, dx \geq -\int_{B_\Gamma} D\frac{(\alpha+1)^2}{2a}\phi|\nabla u|^2 + \frac{6aD}{2\epsilon}|\nabla\phi|(1-\phi)|u|^2 \, dx \tag{52}$$

$$\geq -\int_{B_\Gamma} \phi D|\nabla u|^2 + \frac{3D(\alpha+1)^2}{2\epsilon}|\nabla\phi|(1-\phi)|u|^2 \, dx, \tag{53}$$

where we use $a = (\alpha+1)^2/2$.

For coercivity, we substitute in the inequality above into the B_Γ integral leads to

$$\int_{B_\Gamma} \phi D|\nabla u|^2 + \epsilon^{-2}(1-\phi)|u|^2 + (\alpha+1)u\nabla u \cdot \nabla\phi + \frac{3(\alpha+1)^2}{2\epsilon}(1-\phi)|\nabla\phi||u|^2 \, dx \tag{54}$$

$$\geq \int_{B_\Gamma} \phi D|\nabla u|^2 + \epsilon^{-2}(1-\phi)|u|^2 - \phi D|\nabla u|^2 - \frac{3D(\alpha+1)^2}{2\epsilon}|\nabla\phi|(1-\phi)|u|^2 \tag{55}$$

$$+ \frac{3D(\alpha+1)^2}{2\epsilon}|\nabla\phi|(1-\phi)|u|^2 \, dx$$

$$\geq \int_{B_\Gamma} \epsilon^{-2}(1-\phi)|u|^2 \, dx. \tag{56}$$

□

Remark 2. This NSDDM method has been explored by [37] which shows a coercivity result, and [35], using a different derived values for β. However, our choice of β only impacts the exterior with $(1-\phi)$ and is a direct result from coercivity.

Remark 3. In Appendix A a comparison of these stabilising terms in the Nitsche's method framework will show that, using NDDM is better than the original DDM2 method. Also using the symmetric term in for NSDDM, significantly improves the L^2 error but has a worse H^1 error. It has the obvious property of producing a symmetric matrix, so we will focus on this going forward.

4. Diffuse Domain Mixed Formulation

4.1. Mix0DDM

To derive our new methods we start with the mixed formulation of our model problem (1) given by,

$$\sigma = \nabla u, \tag{57a}$$

$$-\nabla \cdot (D\sigma) = f, \qquad \text{in } \Omega. \tag{57b}$$

$$u = g \qquad \text{on } \partial\Omega. \tag{57c}$$

First we use the weak form of the first equation and integrate by parts to get

$$\int_\Omega \sigma \cdot \tau \, dx = \int_\Omega \nabla u \cdot \tau \, dx = -\int_\Omega u \nabla \cdot \tau \, dx + \int_{\partial\Omega} g\tau \cdot n \, dS. \tag{58}$$

Applying the Diffuse Domain concepts for the weak form approach in section 2.2 this becomes

$$\int_B \phi\sigma \cdot \tau \, dx + \int_B \phi u \nabla \cdot \tau \, dx = \int_B \delta_{\partial\Omega} u\tau \cdot n \, dx = -\int_B g\tau \cdot \nabla\phi \, dx, \tag{59}$$

where we used (8) to obtain $\delta_{\partial\Omega} n = -\nabla\phi$. This is equivalent to

$$\int_B \phi\sigma \cdot \tau \, dx = \int_B \nabla(\phi u) \cdot \tau \, dx - \int_B g\nabla\phi \cdot \tau \, dx. \tag{60}$$

Therefore, we have the following Diffuse Domain approximation for the gradient of u:

$$\phi\sigma = \nabla(\phi u) - g\nabla\phi. \tag{61}$$

Moving to the second equation, we will use an approximation based on strong form approach in section 2.3, since it has the highest convergence rate shown. Therefore, we start with

$$-\phi\nabla \cdot (D\sigma) + \frac{D}{\epsilon^2}(1-\phi)(u-g) = \phi f, \tag{62}$$

and applying the product rule, we obtain

$$-\nabla \cdot (\phi D\sigma) + D\sigma \cdot \nabla\phi + \frac{D}{\epsilon^2}(1-\phi)(u-g) = \phi f. \tag{63}$$

Multiplying by ϕ and substituting equation (61) gives a new method, we will refer to as Mix0DDM:

$$-\phi\nabla \cdot D\left[\nabla(\phi u) - g\nabla\phi\right] + D\left[\nabla(\phi u) - g\nabla\phi\right] \cdot \nabla\phi + \frac{D}{\epsilon^2}(1-\phi)^2(u-g) = \phi^2 f. \tag{64}$$

To make this method coercive, so we add the term

$$\int_B \frac{D}{4}|\nabla\phi|^2(u-g)v \, dx. \tag{65}$$

This leads to the new method,

Method 6 (Mix0DDM). Find $u \in U$ such that

$$a(u,v) := \int_B D\nabla(\phi u) \cdot \left[\nabla(\phi v) + v\nabla\phi\right] + \frac{D}{\epsilon^2}(1-\phi)^2 uv + \frac{D}{4}|\nabla\phi|^2 uv \, dx, \tag{66}$$

$$l(v) := \int_B g\nabla\phi \cdot \left[\nabla(\phi v) + v\nabla\phi\right] + \frac{D}{\epsilon^2}(1-\phi)^2 gv + \frac{D}{4}|\nabla\phi|^2 gv + \phi^2 fv \, dx. \tag{67}$$

For all $v \in V$, where $V = H_0^1(B)$ and $U = V + g$.

For Mix0DDM, we can clearly see this method is not symmetric.

Theorem 5. *Mix0DDM (Method 6) is coercive, with the norm*

$$\|u\|^2 := \int_{B_{int}} |\nabla u|^2 \, dx + \int_{B_{ext}} \epsilon^{-2}|u|^2 \, dx + \int_{B_\Gamma} \epsilon^{-2}(1-\phi)^2|u|^2 \, dx. \tag{68}$$

Proof. The bilinear form with $v = u$ is

$$a(u,u) = \int_B D\nabla(\phi u)\cdot[\nabla(\phi u) + u\nabla\phi] + \frac{D}{\epsilon^2}(1-\phi)^2|u|^2 + \frac{D}{4}|\nabla\phi|^2|u|^2 \, dx. \tag{69}$$

We can see that the $(1-\phi)^2$ term is non-negative, so we will focus on the other terms. To show this method is coercive, we will add a functional zero of $\pm Du\nabla\phi\cdot[\nabla(\phi u) + u\nabla\phi]$. Also, we match corresponding terms in the bilinear form by separating the domain into the same regions in Theorem 2 again.

$$\bar{a}(u,u) = \int_B D\nabla(\phi u)\cdot[\nabla(\phi u) + u\nabla\phi] + \frac{D}{4}|\nabla\phi|^2|u|^2 \, dx, \tag{70}$$

$$= \int_B D|\nabla(\phi u) + u\nabla\phi|^2 - Du\nabla\phi\cdot[\nabla(\phi u) + u\nabla\phi] + \frac{D}{4}|\nabla\phi|^2|u|^2 \, dx. \tag{71}$$

$$= \int_{B_{\text{int}}} D|\nabla u|^2 \, dx. + \int_{B_\Gamma} D|\nabla(\phi u) + u\nabla\phi|^2 + \frac{D}{4}|\nabla\phi|^2|u|^2 - Du\nabla\phi\cdot[\nabla(\phi u) + u\nabla\phi] \, dx. \tag{72}$$

Young's Inequality gives the following bound on the last term,

$$\int_{B_\Gamma} Du\nabla\phi\cdot[\nabla(\phi u) + u\nabla\phi] \, dx \le \frac{1}{2w}\int_{B_\Gamma} D|u\nabla\phi|^2 \, dx + \frac{w}{2}\int_{B_\Gamma} D|\nabla(\phi u) + u\nabla\phi|^2 \, dx. \tag{73}$$

Now the whole bilinear equation becomes

$$a(u,u) \ge \int_{B_{\text{int}}} D|\nabla u|^2 \, dx + \int_{B_\Gamma} \frac{D}{4}|\nabla\phi|^2|u|^2 \, dx + (1-\frac{w}{2})\int_{B_\Gamma} D|\nabla(\phi u) + u\nabla\phi|^2 \, dx - \frac{1}{2w}\int_{B_\Gamma} D|u\nabla\phi|^2 \, dx. \tag{74}$$

Choosing $w = 2$ produces the result,

$$a(u,u) \ge \begin{aligned} &\int_{B_{\text{int}}} D|\nabla u|^2 \, dx + \int_{B_\Gamma} \frac{D}{4}|\nabla\phi|^2|u|^2 - \frac{D}{4}|u|^2|\nabla\phi|^2 + \frac{D}{\epsilon^2}(1-\phi)^2|u|^2 \, dx \\ &\qquad + \int_{B_{\text{ext}}} \frac{D}{\epsilon^2}|u|^2 \, dx. \end{aligned} \tag{75}$$

$$\ge \int_{B_{\text{int}}} D|\nabla u|^2 \, dx + \int_{B_\Gamma} \frac{D}{\epsilon^2}(1-\phi)^2|u|^2 \, dx + \int_{B_{\text{ext}}} \frac{D}{\epsilon^2}|u|^2 \, dx. \tag{76}$$

$$\ge D\left(\int_{B_{\text{int}}} |\nabla u|^2 \, dx + \int_{B_\Gamma} \epsilon^2(1-\phi)^2|u|^2 \, dx + \int_{B_{\text{ext}}} \epsilon^2|u|^2 \, dx\right). \tag{77}$$

Recalling equation (49) for norm used for the Nitsche's Methods Theorem 4, the norm required for Mix0DDM is identical except instead of $(1-\phi)$, we have the $(1-\phi)^2$. Therefore, we can repeat the same proof with the higher power. □

4.2. Mix1DDM

In all the methods we have explored, we enfored $u = g$ in the extended domain B by adding an additional penalization term to the method. We can extend this idea to derive another method where we also enforce $\sigma = \nabla g$ outside the domain.

Recall the interior domain from equation (59),

$$\int_B \phi\sigma \cdot \tau \, dx + \int_B \phi u \nabla \cdot \tau \, dx = -\int_B g_1 \tau \cdot \nabla\phi \, dx. \tag{78}$$

Then complete the same process on the outside to achieve

$$\int_B (1-\phi)\sigma \cdot \tau \, dx + \int_B (1-\phi) g \nabla \cdot \tau \, dx = \int_B g_2 \tau \cdot \nabla\phi \, dx, \tag{79}$$

where the functions g_1, g_2 will be chosen later. Combining these two equations gives,

$$\int_B \sigma \cdot \tau \, dx + \int_B \left[\phi u + (1-\phi) g\right] \nabla \cdot \tau \, dx = \int_B (g_2 - g_1)\tau \cdot \nabla\phi \, dx, \tag{80}$$

which implies the strong form

$$\sigma = \nabla\left[\phi u + (1-\phi) g\right] + (g_2 - g_1)\nabla\phi. \tag{81}$$

Unlike previously in Mix0DDM, we do obtain an equation for σ alone; this allows us to directly substitute σ into the Diffuse Domain formulation of the second equation (62),

$$-\phi\nabla \cdot \left(D\nabla\left[\phi u + (1-\phi) g\right] + (g_2 - g_1)\nabla\phi\right) + \frac{D}{\epsilon^2}(1-\phi)(u-g) = \phi f. \tag{82}$$

Note we have used arbitrary functions g_1 and g_2 because we can use different assumptions on the boundary. We could take $g_1 = g_2 = g$, since we know the Dirichlet boundary conditions match for both regions in the domain. This gives the weak form of equation (82) as

$$\int_B D\nabla\left[\phi u + (1-\phi) g\right] \cdot \nabla(\phi v) + \frac{D}{\epsilon^2}(1-\phi)(u-g) v \, dx = \int_B \phi f v \, dx. \tag{83}$$

For our second method we will take $g_1 = g$ and $g_2 = u$. This can be interpreted as, the interior PDE of u needs to match the Dirichlet boundary g; while the exterior PDE of g needs to match u on the boundary. From experiments this choice of g_1, g_2 performs best, so we will refer to this new method as Mix1DDM.

It is required to add the identical stabilising term from Mix0DDM (65). The weak form of equation (82) becomes

Method 7 (Mix1DDM). Find $u \in U$ such that

$$a(u,v) := \int_B D\left(\nabla(\phi u) + u\nabla\phi\right) \cdot \nabla(\phi v) + \frac{D}{\epsilon^2}(1-\phi) u v + \frac{D}{4}|\nabla\phi|^2 u v \, dx, \tag{84}$$

$$l(v) := \int_B D\left[-\nabla\left[(1-\phi) g\right] + g\nabla\phi\right] \cdot \nabla(\phi v) + \frac{D}{\epsilon^2}(1-\phi) g v + \frac{D}{4}|\nabla\phi|^2 g v + \phi f v \, dx. \tag{85}$$

For all $v \in V$, where $V = H_0^1(B)$ and $U = V + g$.

We can clearly see this is not symmetric.

The only difference in this bilinear form with $v = u$ between Mix1DDM and Mix0DDM is the scaling of the *B.C.* term with $(1-\phi)$. The diffusion terms in both are

$$\int_B D\left[\nabla(\phi u) \cdot \nabla(\phi v) + (u\nabla\phi) \cdot \nabla(\phi v)\right] \, dx$$

Then, for Mix1DDM we have

$$\int_B \frac{D}{\epsilon^2}(1-\phi) u v \, dx$$

instead of with Mix0DDM we have the term

$$\int_B \frac{D}{\epsilon^2}(1-\phi)^2 u v \, dx.$$

Therefore, this will not impact the previous proof for coercivity, that is provided by adding the extra stabilising term. Also, Mix1DDM will use the norm equation (49) in the Nitsche Methods (Theorem 4).

5. Advection-Diffusion Problems

5.1. DDM1/2

As our goal is to apply the Diffuse Domain approach to the Navier-Stokes equations, we will use a splitting method which requires solving the semi-implicit momentum equation as an intermediate step. Therefore, we will first solve advection-diffusion problems. In this section we will focus on the following extension of the Poisson's model equation (1) that we have considered so far:

$$-\nabla \cdot (D\nabla u) + b \cdot \nabla u + mu = f, \quad \text{in } \Omega. \tag{86a}$$

$$u = g \quad \text{on } \partial\Omega, \tag{86b}$$

We have added both a mass term, m, and an advection term with a given velocity vector b. Assuming that this is still an elliptic PDE, we require

$$m - \frac{1}{2}\nabla \cdot b \geq 0 \tag{87}$$

leading to a coercive model.

In [33] it suggests the following Diffuse Domain approximation for the advection term

$$\int_B \phi b \cdot \nabla uv \, dx. \tag{88}$$

This is a straightforward application of the approach described in section 2.3 for DDM2 (Method 2). However, this approximation of the advection term does not guarantee that the resulting bilinear form is positive definite:

Example 1. For simplicity, we will look at a 1D example of our model problem

$$\begin{aligned} -0.0001\frac{d^2}{dx^2}u(x) + \frac{d}{dx}u = 0, \quad x \in [-0.5, 0.5]. \\ u(0.5) = u(-0.5) = 0. \end{aligned}$$

We apply DDM1 for the diffusion and add equation (88) to approximate the advection term on the extended domain $[-0.675, 0.675]$. The signed distance function is given by $r(x) = |x| - 0.5$. Furthermore, we take $\epsilon = 0.035$ and a uniform grid spacing of $h = 0.01$, giving us 7 elements across the interface. The solution is approximated with a linear Lagrange finite element space with the basis $\{\eta_h^i\}$. This means we can construct vectors x for which $x^T Ax = 0$, where A is the system matrix such that $A_{ij} = a(\eta_i, \eta_j)$. For example, fixing an element in the left boundary interface to 1, and selecting another point in the other right interface, then numerically convergence to corresponding x below.

$$x_i = \begin{cases} 1 & \text{if } i = 16 \ (x = -0.515), \\ 0.657218... & \text{if } i = 119 \ (x = 0.515), \\ 0 & \text{otherwise.} \end{cases} \tag{89}$$

To guarantee stability of the method we need to add a stabilising term that takes the difference of the inflow and outflow boundary into account. Focusing first on the advection and mass terms we obtain,

$$\int_\Omega b \cdot \nabla uv + muv \, dx = \int_\Omega \nabla \cdot (bu)v - (\nabla \cdot b)uv + muv \, dx, \tag{90}$$

$$= \int_\Omega -ub \cdot \nabla v + (m - \nabla \cdot b)uv \, dx + \int_{\partial\Omega} b \cdot nuv \, dS. \tag{91}$$

$$= \int_\Omega -ub \cdot \nabla v + (m - \nabla \cdot b)uv \, dx + \int_{\partial\Omega_{\text{out}}} b \cdot nuv \, dS + \int_{\partial\Omega_{\text{in}}} b \cdot nuv \, dS. \tag{92}$$

Note, $\partial\Omega_{\text{in}}$ is the subset of $\partial\Omega$ such that $b \cdot n < 0$ while $\partial\Omega_{\text{out}}$ is subset with $b \cdot n \geq 0$. Motivated by a Nitsche's methods approach for advection [46, 6], we replace u in the final term with g. This can be written as

$$\int_\Omega b \cdot \nabla uv + muv \, dx = \int_\Omega -ub \cdot \nabla v + (m - \nabla \cdot b)uv \, dx + \int_{\partial\Omega} b \cdot nuv \, dS - \int_{\partial\Omega} [b \cdot n]^-(u - g)v \, dS. \quad (93)$$

Therefore, the advection term becomes the following formulation

$$\int_\Omega b \cdot \nabla uv + muv \, dx + \int_{\partial\Omega} [-b \cdot n]^+(u - g)v \, dS, \quad (94)$$

we have used the notation

$$[w]^+ = \begin{cases} w & w > 0 \\ 0 & w < 0 \end{cases}, \qquad \text{and} \qquad [w]^- = \begin{cases} w & w < 0 \\ 0 & w > 0 \end{cases}. \quad (95)$$

Recall that in the Diffuse Domain formulation, we can approximate the normal n by $-\nabla\phi/|\nabla\phi|$. This gives the final integral,

$$\int_{\partial\Omega} [-b \cdot n]^+(u - g)v \, dS \approx \int_B [b \cdot \nabla(\phi)]^+(u - g)v \, . \quad (96)$$

Therefore, a Diffuse Domain approximation to equation (94) is given by

$$\int_B \phi b \cdot \nabla uv + \phi muv + [b \cdot \nabla\phi]^+(u - g)v \, dx. \quad (97)$$

This is identical to equation (88) but with an additional stabilizing term enforcing the boundary conditions on the inflow boundary. From Theorem 1, we know that the sign of $\nabla\phi$ when going from extended domain into the physical domain is positive, and from interior to exterior is negative. Therefore, we can see this is a similar method to the upwind discontinuous Galerkin method [9], and replacing u with g on the inflow boundary.

We thus arrive at the following approximations of the advection-diffusion problem when using DDM1 for the diffusion term:

Method 8 (DDM1 with stabilized advection). Find $u \in U$ such that

$$a(u, v) := \int_B \phi D\nabla u \cdot \nabla v + \frac{D}{\epsilon^3}(1 - \phi)uv + \phi b \cdot \nabla uv + [b \cdot \nabla\phi]^+ uv + \phi muv \, dx, \quad (98)$$

$$l(v) := \int_B \phi f v + \frac{D}{\epsilon^3}(1 - \phi)gv + [b \cdot \nabla\phi]^+ gv \, dx. \quad (99)$$

For all $v \in V$, where $V = H_0^1(B)$ and $U = V + g$.

Theorem 6. *DDM1 with stabilised advection is coercive.*

Proof. As we have already shown coerciveness in Theorem 2 for the diffusion term, we can just focus on the advection term and mass terms

$$\bar{a}(u, v) = \int_B \phi b \cdot \nabla uv + [b \cdot \nabla\phi]^+ uv + \phi muv \, dx \quad (100)$$

for which we need to show that $\bar{a}(u, u) \geq 0$ under the conditions (87) on the data.

We can use integrate by parts on the first term with $u = v$ to give,

$$\int_B \phi b \cdot \nabla uu \, dx = -\int_B \nabla \cdot (\phi bu)u \, dx = \int_B -\nabla \cdot (\phi b)|u|^2 - \phi b \cdot \nabla uu \, dx. \quad (101)$$

Then rearranging and expanding the right-hand side, we get

$$\int_B \phi b \cdot \nabla u u \, dx = \frac{1}{2} \int_B -\nabla \cdot (\phi b) |u|^2 \, dx = \frac{1}{2} \int_B -\phi |u|^2 \nabla \cdot b - |u|^2 b \cdot \nabla \phi \, dx. \tag{102}$$

This means overall we obtain,

$$\bar{a}(u, u) = \int_B -\frac{1}{2} b \cdot \nabla \phi |u|^2 + [b \cdot \nabla \phi]^+ |u|^2 + \phi \left(m - \frac{1}{2} \nabla \cdot b \right) |u|^2 \, dx. \tag{103}$$

From the requirements of the original elliptic PDE, we know this last term is non-negative. We can split the first term into the inflow and outflow boundary regions,

$$\begin{aligned}
\int_B -\frac{1}{2} b \cdot \nabla \phi |u|^2 + [b \cdot \nabla \phi]^+ |u|^2 \, dx &= \int_B \left(-\frac{1}{2} \left[[b \cdot \nabla \phi]^+ + [b \cdot \nabla \phi]^- \right] + [b \cdot \nabla \phi]^+ \right) |u|^2 \, dx && (104) \\
&= \frac{1}{2} \int_B \left([b \cdot \nabla \phi]^+ - [b \cdot \nabla \phi]^- \right) |u|^2 \, dx. && (105) \\
&= \frac{1}{2} \int_B |b \cdot \nabla \phi| |u|^2 \, dx && (106) \\
&\geq 0. && (107)
\end{aligned}$$

As the additional terms are positive, the previous inequality for coercive implies this is also coercive. □

Remark 4. The same argument can be applied to DDM2, NDDM, NSDDM, so we use the same advection and mass terms in equation (100).

5.2. SBM

Following the derivation for the SBM method in Method 3, we multiply the model problem equation (86) by ϕ twice. Thus, this gives the advection and mass term as

$$\int_B \phi^2 b \cdot \nabla u v + \phi^2 m u v \, dx. \tag{108}$$

This is similar to the previous suggestion for DDM1, equation (88), and requires a stabilising term to be added.

Example 2. Taking the previous Example 1 with this advection term, we can construct an example for x such that $x^T A x = 0$. For example,

$$x_i = \begin{cases} 1 & \text{if } i = 16 \ (x = -0.515), \\ 0.975235... & \text{if } i = 119 \ (x = 0.515), \\ 0 & \text{otherwise}, \end{cases} \tag{109}$$

Therefore, we get the following approximation of the elliptic problem using for SBM:

Method 9 (SBM with stabilized advection). Find $u \in U$ such that

$$\begin{aligned}
a(u, v) := \int_B \phi D \nabla u \cdot \nabla(\phi v) + D \nabla \phi \cdot \nabla(\phi u) v + \frac{D}{\epsilon^2}(1 - \phi) u v + \phi^2 b \cdot \nabla u v \\
+ \phi [b \cdot \nabla \phi]^+ u v + \phi^2 m u v \, dx,
\end{aligned} \tag{110}$$

$$l(v) := \int_B \phi^2 f v + D |\nabla \phi|^2 g v + \frac{D}{\epsilon^2}(1 - \phi) g v + \phi [b \cdot \nabla \phi]^+ g v \, dx, \tag{111}$$

for all $v \in V$, where $V = H_0^1(B)$ and $U = V + g$.

Theorem 7. *SBM with stabilised advection is coercive.*

Proof. Here we will closely follow the proof of Theorem 6.

Coerciveness has already been shown for the diffusion term in Theorem 3, so we will focus on the advection term and mass terms:

$$\bar{a}(u,v) = \int_B \phi^2 b \cdot \nabla u v + \phi[b\cdot\nabla\phi]^+ uv + \phi^2 m u v \, dx. \tag{112}$$

We need to show that $\bar{a}(u,u) \geq 0$ under the conditions (87) on the data.

Using the same integrate by parts on the first term and rearranging with $u = v$ gives,

$$\int_B \phi^2 b\cdot\nabla u u \, dx = \frac{1}{2}\int_B -\phi^2|u|^2\nabla\cdot b - |u|^2 b\cdot\nabla(\phi^2)\, dx. = \int_B -\frac{1}{2}\phi^2|u|^2\nabla\cdot b - |u|^2 b\cdot\nabla\phi\phi \, dx. \tag{113}$$

So that overall we obtain,

$$\bar{a}(u,u) = \int_B -\phi b\cdot\nabla\phi|u|^2 + \phi[b\cdot\nabla\phi]^+|u|^2 + \phi^2\left(m - \frac{1}{2}\nabla\cdot b\right)|u|^2\, dx. \tag{114}$$

The original elliptic PDE requirements show this last term is non-negative. Focusing on the first term, we can split this into the inflow and outflow boundary regions,

$$\begin{aligned}
\int_B -\phi b\cdot\nabla\phi|u|^2 + \phi[b\cdot\nabla\phi]^+|u|^2\, dx &= \int_B \phi\left(-\frac{1}{2}\left[[b\cdot\nabla\phi]^+ + [b\cdot\nabla\phi]^-\right] + [b\cdot\nabla\phi]^+\right)|u|^2\, dx && (115)\\
&= \frac{1}{2}\int_B \phi|b\cdot\nabla\phi||u|^2\, dx && (116)\\
&\geq 0. && (117)
\end{aligned}$$

Similarly, this shows the stabilising term is needed for coerciveness. □

5.3. Mix0DDM

For the mixed methods, we again consider the mixed formulation of our problem

$$\begin{aligned}
\sigma &= \nabla u, & -\nabla\cdot\sigma + b\cdot\sigma + mu &= f, & \text{in } \Omega. && (118)\\
u &= g & \text{on } \partial\Omega. & && && (119)
\end{aligned}$$

Recall, in Mix0DDM we obtained the Diffuse Domain approximation for σ of the form $\phi\sigma = \nabla(\phi u) - g\nabla\phi$. Then we needed to multiply the second equation with ϕ^2. Consequently, the Mix0DDM approximation of the advection term is given by

$$\int_B \phi^2 b\cdot\sigma v\, dx = \int_B \phi b\cdot(\nabla(\phi u) - g\nabla\phi)\, v\, dx. \tag{120}$$

This gives the following method:

Method 10 (Mix0DDM with advection). Find $u \in U$ such that

$$\begin{aligned}
a(u,v) &:= \int_B D\nabla(\phi u)\cdot[\nabla(\phi v) + v\nabla\phi] + \frac{D}{\epsilon^2}(1-\phi)^2 uv + \frac{D}{4}|\nabla\phi|^2 uv + \phi b\cdot\nabla(\phi u)v + \phi^2 m u v\, dx, && (121)\\
l(v) &:= \int_B g\nabla\phi\cdot[\nabla(\phi v) + v\nabla\phi] + \frac{D}{\epsilon^2}(1-\phi)^2 g v + \frac{D}{4}|\nabla\phi|^2 g v + \phi b\cdot g\nabla\phi v + \phi^2 f v\, dx. && (122)
\end{aligned}$$

For all $v \in V$, where $V = H_0^1(B)$ and $U = V + g$.

Note, we do not have to add any special treatment for the inflow boundary, as we can show that the terms added for the advection are already coercive.

Theorem 8. *Mix0DDM with advection is coercive.*

PROOF. We can rearrange the advection term in the bilinear form with $v = u$:

$$\int_B \phi b \cdot \nabla(\phi u) u \, dx = -\int_B \phi^2 \nabla \cdot b |u|^2 + \phi b \cdot \nabla(\phi u) u \, dx. \tag{123}$$

Therefore, the advection and mass term become

$$\int_B \phi b \cdot \nabla(\phi u) u + \phi^2 m |u|^2 \, dx = \int_B \phi^2 \left(m - \frac{1}{2} \nabla \cdot b \right) |u|^2 \, dx \geq 0. \tag{124}$$

This is non-negative, using the assumptions on the data of the PDE, so the advection term is positive semi-definite. Therefore, combining this with Theorem 5, we see the Mix0DDM with advection is stable. □

5.4. Mix1DDM

For Mix1DDM where $\sigma = \nabla[\phi u + (1-\phi)g] + (u-g)\nabla\phi$ is used, we do need to add a stabilising term on the outflow boundary to obtain a stable scheme:

Method 11 (Mix1DDM with advection). Find $u \in U$ such that

$$\begin{aligned} a(u,v) := \int_B [\nabla(\phi u) + u \nabla \phi] \cdot [D \nabla(\phi v) + \phi b v] + \frac{D}{\epsilon^2}(1-\phi) u v + \frac{D}{4} |\nabla \phi|^2 u v \\ - \phi [b \cdot \nabla \phi]^- u v + \phi m u v \, dx, \end{aligned} \tag{125}$$

$$\begin{aligned} l(v) := \int_B [-\nabla [(1-\phi) g] + g \nabla \phi] \cdot [D \nabla(\phi v) + \phi b v] + \frac{D}{\epsilon^2}(1-\phi) g v + \frac{D}{4} |\nabla \phi|^2 g v \\ + \phi f v - \phi [b \cdot \nabla \phi]^- g v \, dx. \end{aligned} \tag{126}$$

For all $v \in V$, where $V = H_0^1(B)$ and $U = V + g$.

Theorem 9. *Mix1DDM with advection is coercive.*

PROOF. First, we can expand the (non stabilised) advection term in the bilinear form and then follow similar steps to the previous Theorem 8.

$$\int_B \phi b \cdot [u \nabla(\phi) + \phi \nabla(u) + u \nabla \phi] \, u \, dx, \tag{127}$$

$$= 2 \int_B \phi b \cdot \nabla \phi |u|^2 \, dx + \int_B \phi^2 b \cdot \nabla u u \, dx, \tag{128}$$

$$= 2 \int_B \phi b \cdot \nabla \phi |u|^2 \, dx + \int_B \frac{1}{2} \phi^2 b \cdot \nabla(u^2) \, dx. \tag{129}$$

Continuing by using integrate by parts and product rule,

$$= 2 \int_B \phi b \cdot \nabla \phi |u|^2 \, dx - \frac{1}{2} \int_B \phi^2 \nabla \cdot b |u|^2 + 2\phi b \cdot \nabla \phi |u|^2 \, dx, \tag{130}$$

$$= \int_B \phi b \cdot \nabla \phi |u|^2 \, dx - \frac{1}{2} \int_B \phi^2 \nabla \cdot b |u|^2 \, dx. \tag{131}$$

Therefore, the advection and mass terms in the bilinear form with $u = v$ are equivalent to

$$\int_B \phi b \cdot [\nabla(\phi u) + u\nabla\phi]\, u - \phi[b \cdot \nabla\phi]^- |u|^2 + \phi m|u|^2 \, dx, \tag{132}$$

$$= \int_B \phi b \cdot \nabla\phi|u|^2 - \frac{1}{2}\phi^2\nabla \cdot b|u|^2 - \phi[b \cdot \nabla\phi]^- |u|^2 + \phi m|u|^2 \, dx. \tag{133}$$

Since $\phi \in (0, 1)$ we have $\phi^2 < \phi$ and consequently,

$$\int_B \phi^2 \left(m - \frac{1}{2}\nabla \cdot b\right) |u|^2 \, dx \geq 0. \tag{134}$$

Then, we can split the first term into the inflow and outflow directions

$$\int_B \phi b \cdot \nabla\phi|u|^2 - \phi[b \cdot \nabla\phi]^- |u|^2 \, dx, = \int_B \phi \left[[b \cdot \nabla\phi]^+ + [b \cdot \nabla\phi]^- - [b \cdot \nabla\phi]^-\right] |u|^2 \, dx, \tag{135}$$

$$= \int_B \phi[b \cdot \nabla\phi]^+ |u|^2 \, dx \tag{136}$$

$$\geq 0. \tag{137}$$

So we obtain a coercive bilinear form for Mix1DDM with advection. □

6. Numerical Experiments

We will now look at some numerical experiments of the new methods to evaluate their potential. These will be implemented in Python using the package DDFEM [7], with meshes generated with `Gmsh` [19] and DUNE-ALUGRID [4], and solved using DUNE-FEM [44, 15]. First we shall focus on the Advection-Diffusion model problem in equation (86), using the Lagrange space on triangles. The goal is to apply these methods to Navier-Stokes, where we will use the Taylor-Hood space, so we need to test both first and second order basis functions. Initially we will solve the corresponding matrix system directly to ensure errors are only from the approximations. This allows an exact manufactured solution to be constructed, while varying arguments will show source of error.

To compute the error we use

$$E_{L^2} = \|\chi_\Omega(u - u_h)\|_{L^2}, \tag{138}$$

$$E_{H^1} = \|\chi_\Omega(u - u_h)\|_{H^1} = \begin{cases} E_{L^2} + \|\chi_\Omega(\nabla u - \sigma_h)\|_{L^2} & \text{Mix0DDM or Mix1DDM}, \\ E_{L^2} + \|\chi_\Omega(\nabla u - \nabla u_h)\|_{L^2} & \text{otherwise}. \end{cases} \tag{139}$$

Note, the interface width is always chosen such that it will contain at least 7 elements i.e., $2\epsilon = 7h$.

Here we will focus at the best two methods, but the full results are contained within Appendix A. All our numerical experiments show that the original or stabilised DDM1 (Method 8) and DDM2 (Method 2) are outperformed by the new methods in the L^2 norm.

6.1. Advection-Diffusion Problems

Initially we take the advection term $b = (0, 0)$, to see the accuracy of the diffusion and boundary term. Also, we take the non-constant scalar diffusion coefficient,

$$-\nabla \cdot [(1 + |x|)\nabla u] = f, \tag{140}$$

where f is constructed such that we have the exact solution

$$u(x) = \cos(1.8\pi x_1) \cos(2.6\pi x_2). \tag{141}$$

Two domains will be used: a smooth arc shape extended into a simple square with a width 7ϵ larger than outer radius; and an inverted domain, which has the arc cutout from a square, with the fixed amount extended inside the arc. For convergence tests it is required to start with a mesh size small enough to ensure the new external boundary conditions do not impact the results. An example of this domain is shown in figure 1, and a sign distance function can be derived from [40]. The use of DDFEM allows complex domains to easily be defined by combining sign distance function, which is demonstrated in [7].

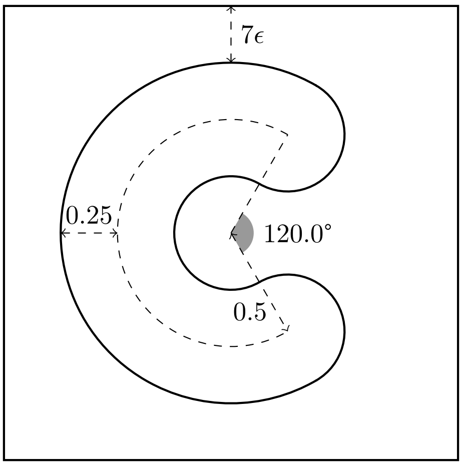

Figure 1: Arc shape domain.

These results are shown in figures 2 and 3. NSDDM (Method 5) almost always has the best L^2 errors,

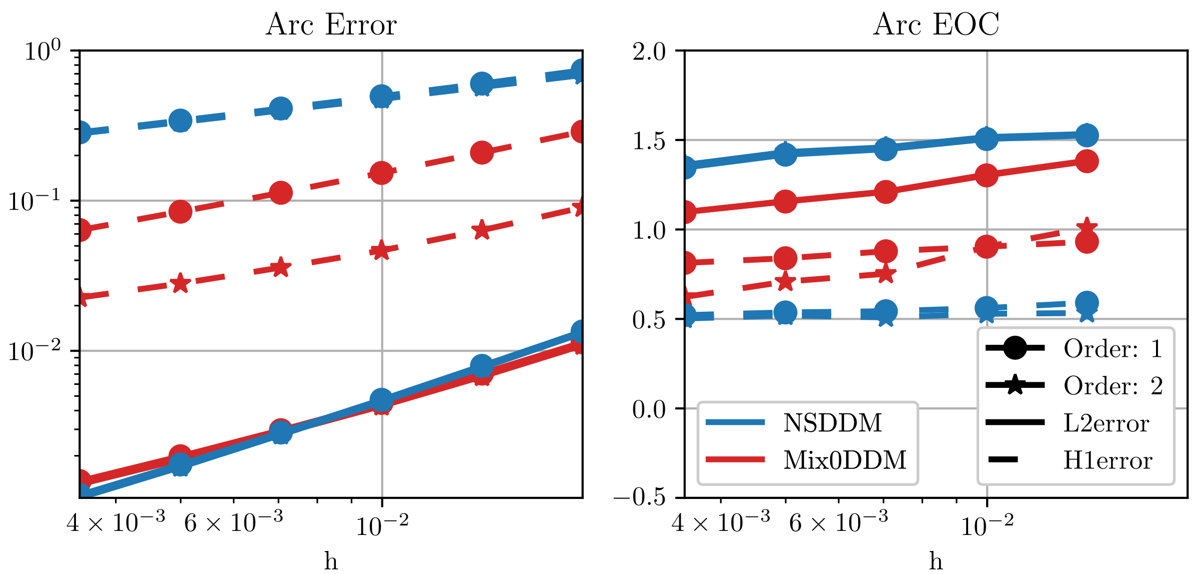

Figure 2: Diffusion Dominated problem error plot for Arc domain.

which is closely followed by Mix0DDM (Method 6). These will be a useful combination of methods to focus on to limit the combination of parameters, as this explores the new mixed methods and our version using Nitsche's method. This means we have a symmetric method that offers a high accuracy L^2 error, which would be beneficial for certain problems, for example the Stokes fluid flow.

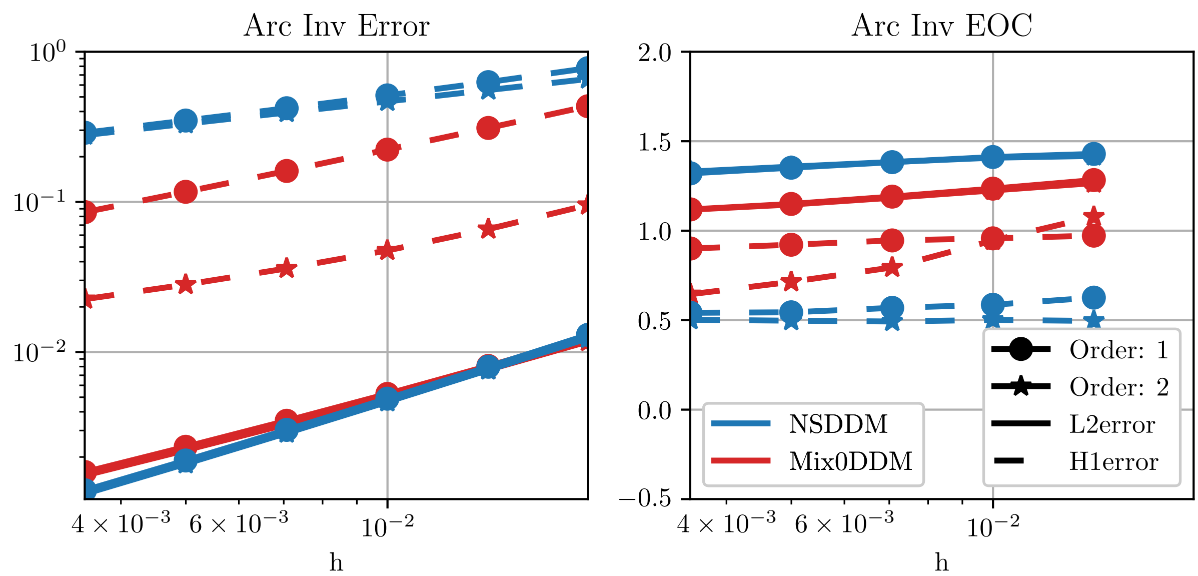

Figure 3: Diffusion Dominated problem error plot for Inverted Arc domain.

In the H^1 errors Mix0DDM preforms the best, and closely followed by Mix1DDM. However, NSDDM preforms worse than other methods, this means a compromise of the symmetric property and H^1 needs to be considered depending on the problem. Furthermore, the second order results show that the H^1 errors for Mix0DDM are improved as well. NSDDM is not significantly impacted from increasing basis order.

We follow the same experiments but increase the advection term significant to investigate the errors for an advection dominate problem,

$$-\nabla \cdot [(1 + |x|)\nabla u] - 100 \begin{bmatrix} x_2 \\ x_1 \end{bmatrix} \cdot \nabla u = f. \tag{142}$$

In figures 4 and 5 we can see a very similar outcome to the case without advection. Again Mix0DDM performs only slightly worse in the L^2-norm compared to NSDDM with no advantage of using a second order space. While as before there is a clear difference in the H^1-norm between the two methods with Mix0DDM showing a higher EOC then NSDDM.

6.2. Searchlight Advection Problem

To further evaluate the performance of the methods for advection dominated problems, we will look at

$$-D\Delta u - \begin{bmatrix} -x_1 \\ x_0 \end{bmatrix} \cdot \nabla u = 0. \tag{143a}$$

$$u = \begin{cases} 0.5 & 0.35 < |x| < 0.65 \text{ and } x_1 > 0 \\ -0.5 & \text{otherwise} \end{cases} \quad \text{on } \partial\Omega. \tag{143b}$$

The problem is shown in figure 6: the green part of the boundary shows the inflow and black is characteristic or outflow. While we don't have an exact solution for this problem, this figure shows an approximation of the expected solution given $D = 0$.

To evaluate the results with $D = 10^{-3}$, we can sample across the yellow line in the figure, with end points $[-0.7, -0.8]$ and $[0.1, 0.8]$. The results are shown in figure 7 with two different spatial resolution. Both methods converge to the expected result with Mix0DDM preforming better, especially in the downwind part of the domain (left side of the plots).

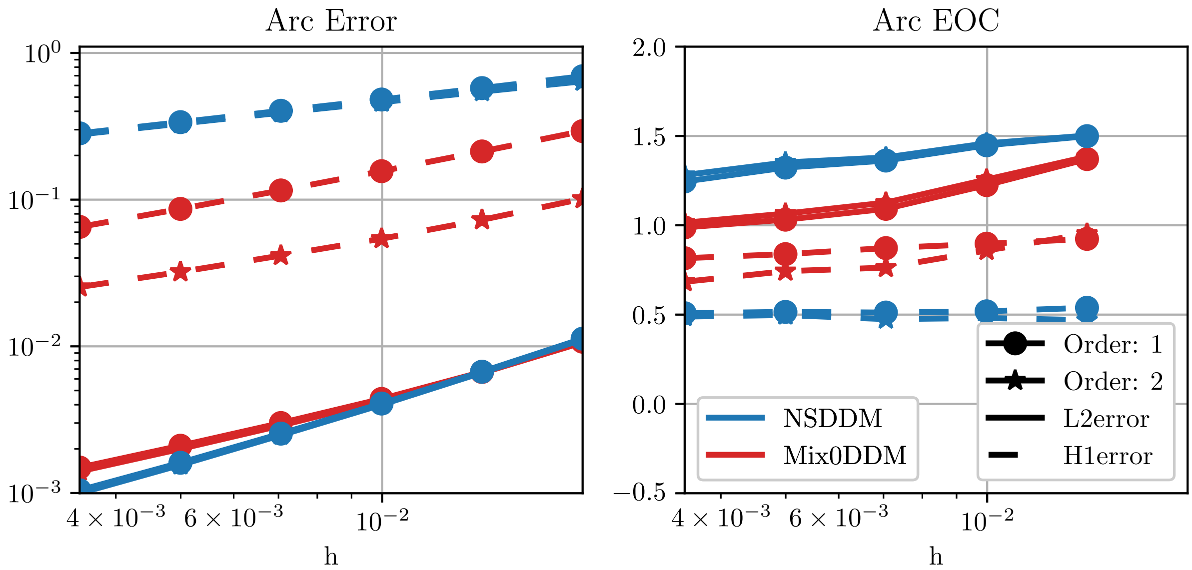

Figure 4: Advection Dominated problem error plot for Arc domain.

The results in figure 8 and figure 9, show a significant difference between the methods on the coarser mesh. With Mix0DDM preforming significantly better, although showing some oscillations at the outflow boundary. The fine mesh shows similar results, there is still a significant difference at the outflow boundary. NSDDM clearly enforces $u = -0.5$ more strongly but with a larger than expected boundary layer. Mix0DDM seems to produce a very thin layer and not resolving $u = -0.5$, more similar to what is seen in discontinuous Galerkin methods.

6.3. Incompressible Navier-Stokes

Finally, we have reached our goal of the incompressible Navier-Stokes problem. We will solve this using incremental pressure correction (IPC) which is a second-order projection scheme from [23, 22]. Note, a simpler Diffuse Domain projection method has been used in [3]. The key benefit of this method is to decouple the velocity and pressure, so they are solved independently. We compute a tentative velocity by removing the current pressure term in the momentum equation and divergence free constraint. For a time step of τ, we solve the following for $\tilde{u}$

$$\frac{3\tilde{u} - 4u^n + u^{n-1}}{2\tau} - \nu\Delta\tilde{u} + (u_\star^{n+1}\cdot\nabla)\tilde{u} = f^{n+1} - \nabla p^n, \tag{144a}$$

$$u = g \quad \text{on } \partial\Omega, \tag{144b}$$

where $u_\star^{n+1} = 2u^n - u^{n-1}$. Then using the Helmholtz decomposition, the tentative velocity is projected into the divergence free space. Giving the two equations to solve: First solving for $\tilde{p}$,

$$-\Delta\tilde{p} = -\frac{3}{2\tau}\nabla\cdot\tilde{u}, \tag{145a}$$

$$\nabla\tilde{p}\cdot n = 0 \quad \text{on } \partial\Omega, \tag{145b}$$

where $\tilde{p} = p^{n+1} - p^n$. Then solving, u^{n+1}

$$u^{n+1} = \tilde{u} - \frac{2\tau}{3}\nabla\tilde{p}. \tag{146}$$

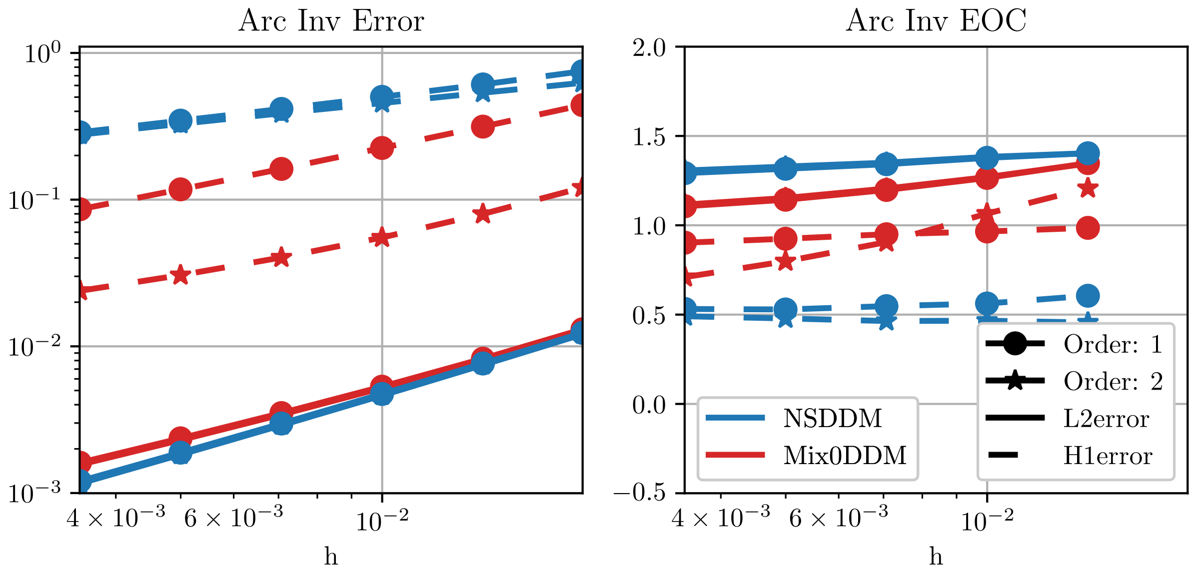

Figure 5: Advection Dominated problem error plot for Inverted Arc domain.

Note due to the uncoupling, this introduces a splitting error of order $\mathcal{O}(\tau^2)$, so there is no improvement to using a higher order discretization in time [27, Section 7.5].

To solve this problem in the Diffuse Domain approach we use the components previously introduced. Although, due to the advection term being divergence free, in DDFEM the advection has been implemented as a source term. To incorporate new terms for gradients and divergence. For the gradient, we can follow the same approach as the mass term,

$$\int_\Omega \nabla p \cdot v \, dx \approx \int_B \phi \nabla p \cdot v \, dx. \tag{147}$$

Recall, Mix0DDM (8) and SBM (7) both require multiplying by ϕ^2.

In equation (145) we require the Neumann boundary condition, these are introduced in [33, 31]. The following problems require homogeneous boundary conditions, so the term disappears from the equation. For example, changing the boundary conditions on the model problem equation (1),

$$-\nabla \cdot (D\nabla p) = f \quad \text{in } \Omega, \tag{148a}$$
$$\nabla p \cdot n = p_N \quad \text{on } \partial\Omega, \tag{148b}$$

the Diffuse Domain problem becomes,

$$-\nabla \cdot (\phi D \nabla p) + p_N |\nabla \phi| = \phi f. \tag{149}$$

Therefore, as the Neumann boundary condition use the weak approach, we apply that approach to the divergence term.

$$0 = \int_\Omega \nabla \cdot uq \, dx = \int_\Omega u \cdot \nabla q \, dx - \int_{\partial\Omega} g \cdot nq \, dS \approx \int_B \phi u \cdot \nabla q + g \cdot \nabla \phi q \, dx \tag{150}$$

This is implemented in DDFEM as an advection term for the pressure, and using the DDM1 method.

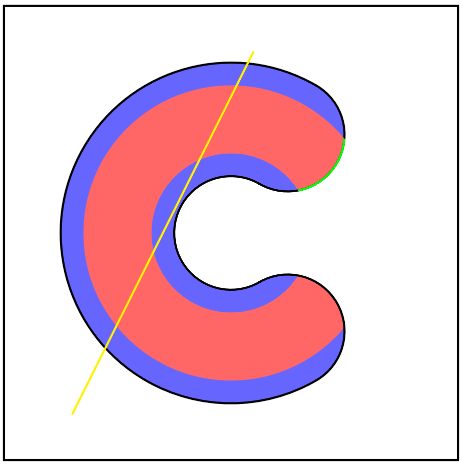

Figure 6: Solution for searchlight with arc domain.

6.3.1. Taylor-Green Vortex

The Taylor-Green vortex is a manufactured solution for Navier-Stokes, so we have an exact solution [48]. Following the example in [34], we have the exact solution

$$u(t,x) = \left(-\cos(2\pi x_1)\sin(2\pi x_2)e^{-8\pi^2\nu t}, sin(2\pi x_1)\cos(2\pi x_2)e^{-8\pi^2\nu t}\right)^T,$$
$$p(t,x) = -\frac{1}{4}(\cos(4\pi x_1)+\cos(4\pi x_2))e^{-16\pi^2\nu t}.$$

This gives $f = 0$, and we will select $\nu = 0.01$ to solve on the domain of a ball with a 0.5 radius, $\Omega = B_{0.5}(0)$.

For this problem, we will look at the errors across time using the following errors [47],

$$E_{L^2}(u_h) = \left(\sum_n \tau\|\chi_\Omega(u(t_n) - u_h^n)\|_{L^2}^2\right)^{\frac{1}{2}},$$
$$E_{H^1}(u_h) = \left(\sum_n \tau\|\chi_\Omega(u(t_n) - u_h)\|_{H^1}^2\right)^{\frac{1}{2}},$$
$$E_{L^2}(p_h) = \left(\sum_n \tau\|\chi_\Omega(p(t_n) - p_h^n)\|_{L^2}^2\right)^{\frac{1}{2}}.$$

The results for NSDDM are shown in table 1 and Mix0DDM are shown in table 2. Note we don't expect the pressure error to match exactly as it is solved uniquely up to a constant. The results have been shifted to the closest match, showing the magnitude of the errors between the methods is the same, by NSDDM showing a higher convergence rate.

We can see both methods have the velocity converging to the correct solution and have similar error magnitude to the previous experiments in section 6.1 The L^2 EOCs preform similar to those experiments, with Mix0DDM performing close to NSDDM; although both EOCs fall short of the theoretical possible for Taylor-Green. This suggests the Diffuse Domain error is dominating. The most significant difference appears in the H^1 error, with Mix0DDM performing better in convergence rates and absolute value.

6.3.2. Flow Around a Cylinder

Focusing on the Kármán vortex street case from the DFG 2D-3 benchmark [45]. This problem consists of the flow through a domain $\Omega = [0, 2.2]\times[0, 4.1]\backslash B_{0.05}(0.2, 0.2)$, which will extend to remove the cylinder from

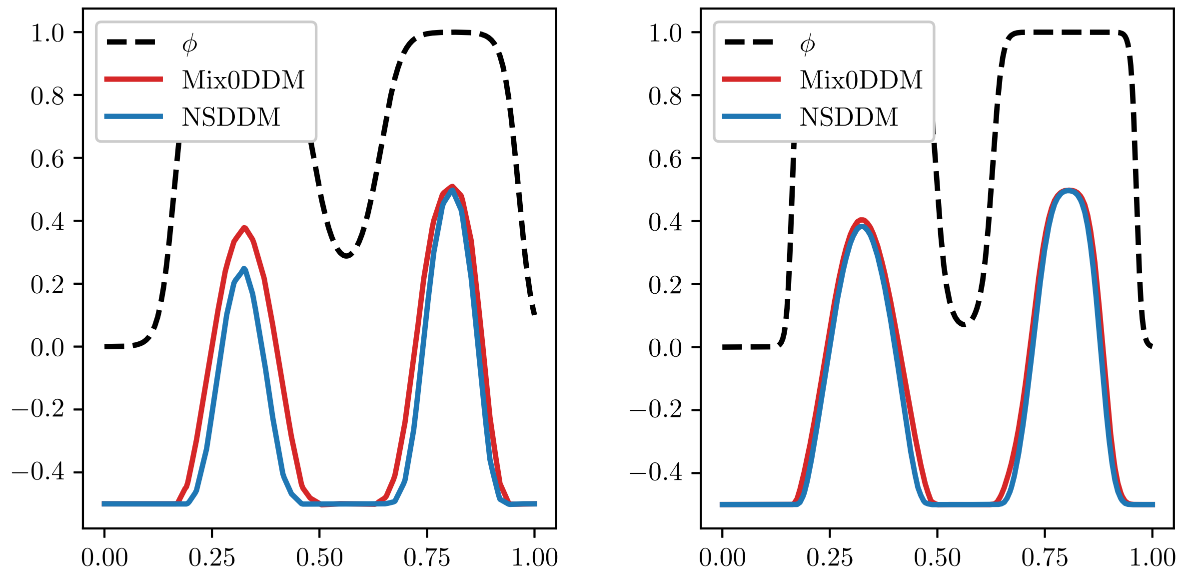

(a) $h = 0.04988$

(b) $h = 0.01761$

Figure 7: Advection problem sample for Arc domain.

the mesh. This is shown in figure 10. The problem has $\nu = 0.001$, and the following boundary conditions: the time dependent Dirichlet inflow boundary

$$u(t,(0,x_2)) = \left(\frac{6x_2(0.41-x_2)}{0.41^2}\sin\left(\frac{\pi t}{8}\right), 0\right)^T \qquad \forall x_2 \in [0, 0.41],$$

a do-nothing outflow boundary

$$(\nabla u n - pI)n = 0,$$

and the other boundaries have a no slip boundary

$$u = 0.$$

The do-nothing boundary condition is the exterior boundary condition and far away from the extended region, therefore, it will not have an impact on the Diffuse Domain approximation.

h	$E_{L^2}(u_h)$	$E_{L^2}(u_h)$ EOC	$E_{H^1}(u_h)$	$E_{H^1}(u_h)$ EOC	$E_{L^2}(p_h)$	$E_{L^2}(p_h)$ EOC
5.00×10^{-2}	2.12×10^{-2}	-	5.55×10^{-1}	-	8.70×10^{-3}	-
3.54×10^{-2}	1.35×10^{-2}	1.29	4.63×10^{-1}	0.52	5.23×10^{-3}	1.46
2.50×10^{-2}	8.57×10^{-3}	1.32	3.96×10^{-1}	0.45	3.01×10^{-3}	1.59
1.77×10^{-2}	5.39×10^{-3}	1.34	3.41×10^{-1}	0.43	1.67×10^{-3}	1.71
1.25×10^{-2}	3.35×10^{-3}	1.37	2.92×10^{-1}	0.45	8.95×10^{-4}	1.79
8.84×10^{-3}	2.09×10^{-3}	1.35	2.50×10^{-1}	0.45	4.77×10^{-4}	1.81

Table 1: NSDDM method error for Taylor-Green problem.

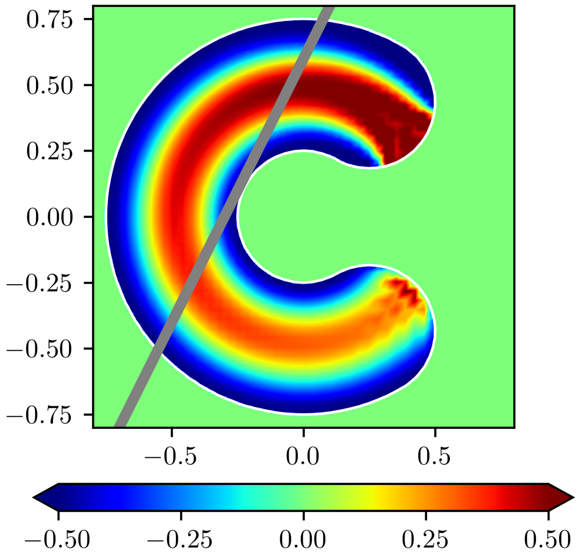

(a) $h = 0.04988$

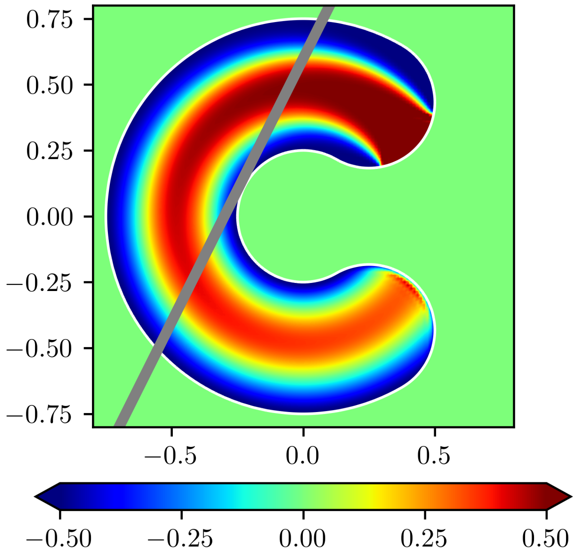

(b) $h = 0.01761$

Figure 8: Contour plots of Mix0DDM approximation solutions for Arc domain.

h	$E_{L^2}(u_h)$	$E_{L^2}(u_h)$ EOC	$E_{H^1}(u_h)$	$E_{H^1}(u_h)$ EOC	$E_{L^2}(p_h)$	$E_{L^2}(p_h)$ EOC
5.00×10^{-2}	2.09×10^{-2}	-	2.47×10^{-1}	-	6.69×10^{-3}	-
3.54×10^{-2}	1.30×10^{-2}	1.37	1.56×10^{-1}	1.33	3.99×10^{-3}	1.49
2.50×10^{-2}	8.22×10^{-3}	1.32	9.87×10^{-2}	1.32	2.31×10^{-3}	1.58
1.77×10^{-2}	5.23×10^{-3}	1.30	6.37×10^{-2}	1.26	1.29×10^{-3}	1.67
1.25×10^{-2}	3.32×10^{-3}	1.31	4.25×10^{-2}	1.17	7.26×10^{-4}	1.66
8.84×10^{-3}	2.15×10^{-3}	1.25	3.03×10^{-2}	0.97	4.32×10^{-4}	1.50

Table 2: Mix0DDM method error for Taylor-Green problem.

During the experiments we measure three quantities of interest [29, 25]: drag coefficient, $c_d(t)$, lift coefficient, $c_l(t)$, and the pressure difference around the cylinder,

$$\Delta p(t) = p(t, (0.15, 0.2)) - p(t, (0.25, 0.2)).$$

These coefficients are derived from

$$\begin{pmatrix} C_d \\ C_l \end{pmatrix} = \frac{2}{\rho L U_{\text{mean}}^2} \int_{\partial\Omega} (\nu \nabla u - pI) n \, dS.$$

This can be easily converted into an integral that we can compute in the Diffuse Domain framework; we have the extended normal defined Definition 3 and the surface delta in equation (8).

$$\begin{pmatrix} C_d \\ C_l \end{pmatrix} \approx \frac{2}{\rho L U_{\text{mean}}^2} \int_{B} (pI - \nu \nabla u) \nabla \phi \, dx.$$

Using a refined mesh such that, the largest elements have a diameter of $h_{max} = 0.02$ and the diameter

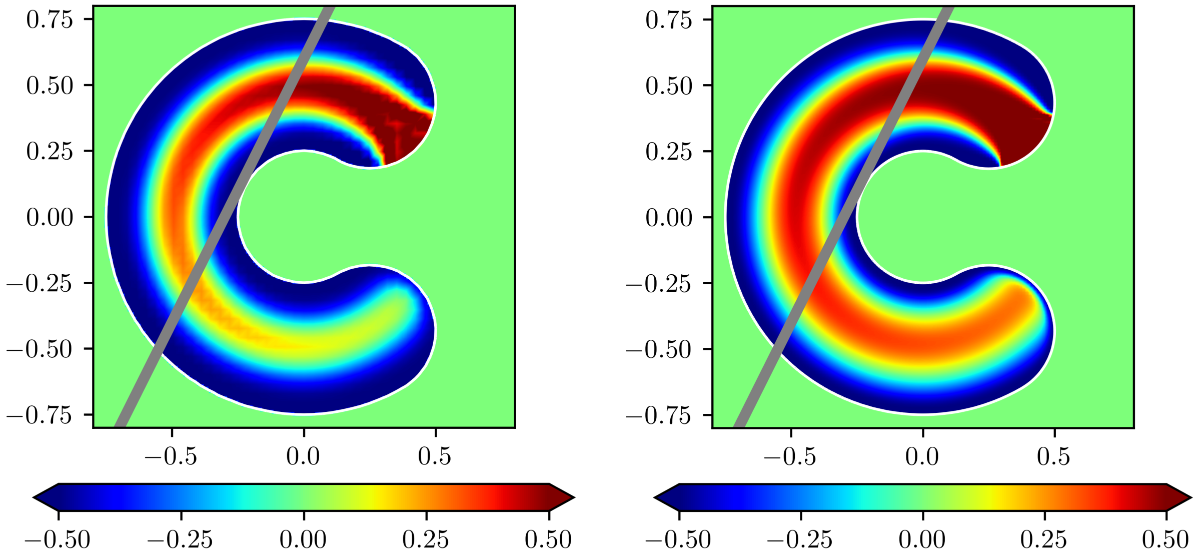

(a) $h = 0.04988$

(b) $h = 0.01761$

Figure 9: Contour plots of NSDDM approximation solutions for Arc domain.

Figure 10: Cylinder Flow Domain

of the smallest elements is $h_{min} = 0.005$. The element size increases linearly, starting at a distance of $5\epsilon = 0.0875$ from the interface of the cylinder, reaching the largest size at $20\epsilon = 0.35$.

To ensure numerical stability and reduce time step errors, we set $\tau = 0.005$. This gives the results for the chosen measurements in figure 11. To evaluate the accuracy of these results in table 3 they are compared against the experiments performed by John [26], and the simulations were run with the same IPC method on a similarly refined, fitted mesh.

From the lift coefficient measurements, it is clear both methods produce the expected vortex shedding with alternating lift. Also, the maximums occur close to the reference time, however they are producing a greater lift; with NSDDM preforming slightly better. A similar behaviour can be spotted in the drag coefficient, with both methods producing the maximum value close to the expected time. However, both methods have a noticeable difference from the expected drag coefficient. The maximum drag for NSDDM undershot the reference value, and overshot the reference value for Mix0DDM. Finally, comparing the pressure difference we can see both methods produce very close results on the figure, which is similar to the performance shown for the Taylor-Green problem.

Method	$t(C_{d,\max})$	$C_{d,\max}$	$t(C_{l,\max})$	$C_{l,\max}$	$\Delta p(8\mathrm{s})$
John [26]	3.93625	2.950921575	5.693125	0.47795	-0.1116
Fitted	3.93500	2.9247938	5.47500	0.4328733	-0.1107880
Mix0DDM	3.96000	3.0790530	5.57500	0.7213531	-0.0946709
NSDDM	3.96000	2.7449023	5.58500	0.6855609	-0.0923733

Table 3: Reference value comparison for measurements of flow Navier-Stokes around cylinder.

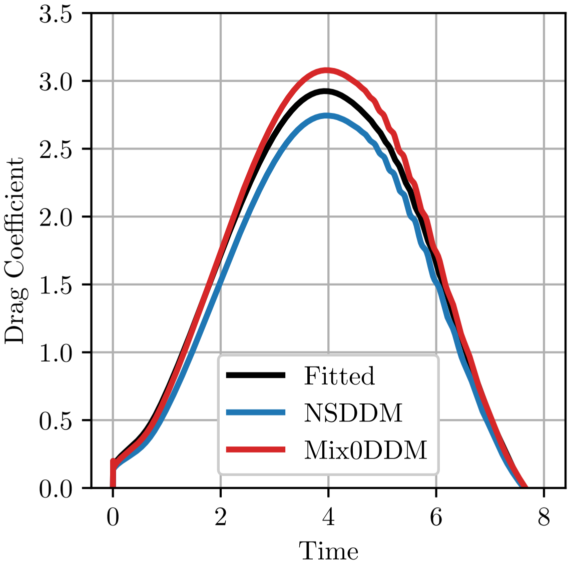

(a) Drag coefficient.

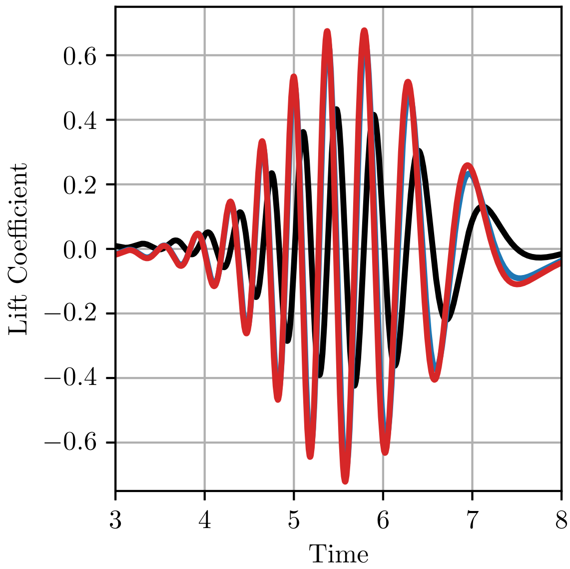

(b) Lift coefficient

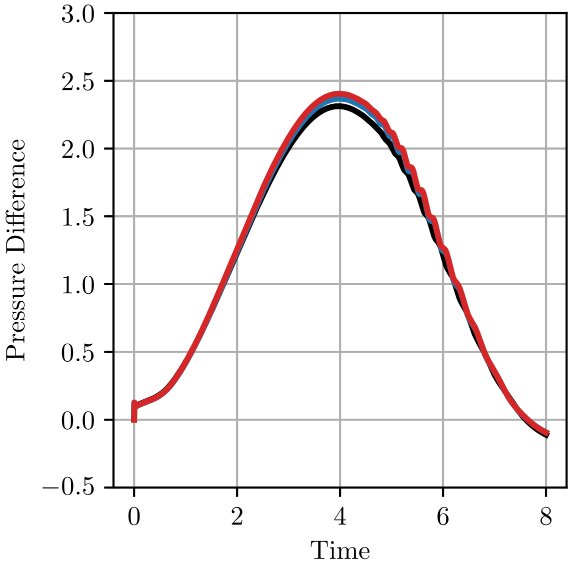

(c) Pressure difference

Figure 11: Measurements for Navier-Stokes flow around cylinder.

7. Conclusion

We have introduced and analysed a new approach for applying the Diffuse Domain method to partial differential equations on complex domains, derived from a mixed formulation. This led to the development of two new methods, Mix0DDM and Mix1DDM. A key benefit of these methods, for certain problems, is that it transforms the essential Dirichlet boundary conditions into natural boundary conditions within the gradient equation of the mixed system. Furthermore, we derived new stabilised methods derived from Nitsche's method, NSDDM and NDDM, and improved stabilisation of existing methods.

Numerical experiments for Advection-Diffusion problems demonstrated that the new methods improve on the existing methods. NSDDM, consistently produced the best L^2 error, and while Mix0DDM performed close in the L^2 error, it performed significantly better in the H^1 error. This suggests that Mix0DDM is especially beneficial for problems where the accuracy of the solution's gradient is important, due to the boundary conditions being included in $\sigma \approx \nabla u$.

Notably, Mix0DDM method was the only method proven to be coercive without an additional stabilisation term, whereas NSDDM is a high performing symmetric formulation.

The experiments of the incompressible Navier-Stokes equations, using an incremental pressure correction scheme, demonstrated their accuracy for complex Dirichlet boundary problems. Both methods produced the expected behaviour, however, the measurements showed some error relative to the reference values.

Future work should focus on a rigorous asymptotic analysis of the new methods to establish their theoretical convergence rates, and calculate optimal choice of ϵ scaling in $B.C.$ terms.

References

[1] Abels, H., Lam, K.F., Stinner, B., 2015. Analysis of the diffuse domain approach for a bulk-surface coupled pde system. SIAM Journal on Mathematical Analysis 47, 3687–3725. doi:10.1137/15m1009093.

[2] Aland, S., Landsberg, C., Müller, R., Stenger, F., Bobeth, M., Langheinrich, A., Voigt, A., 2012. Adaptive diffuse domain approach for calculating mechanically induced deformation of trabecular bone. Computer Methods in Biomechanics and Biomedical Engineering 17, 31–38. doi:10.1080/10255842.2012.654606.

[3] Aland, S., Lowengrub, J., Voigt, A., 2010. Two-phase flow in complex geometries: A diffuse domain approach. Computer Modeling in Engineering & Sciences 57, 77–106. doi:10.3970/cmes.2010.057.077.

[4] Alkämper, M., Dedner, A., Klöfkorn, R., Nolte, M., 2016. The dune-alugrid module. Archive of Numerical Software 4, 1–28. doi:10.11588/ANS.2016.1.23252.

[5] Anderson, D.M., McFadden, G.B., Wheeler, A.A., 1998. Diffuse-Interface Methods in Fluid Mechanics. Annual Review of Fluid Mechanics 30, 139–165. doi:10.1146/annurev.fluid.30.1.139.

[6] Bazilevs, Y., Hughes, J.J.R., 2007. Weak imposition of dirichlet boundary conditions in fluid mechanics. Computers & Fluids 36, 12–26. doi:10.1016/j.compfluid.2005.07.012.

[7] Benfield, L., Dedner, A., 2025. Ddfem: A python package for diffuse domain methods. arXiv:2507.16964.

[8] Benzaken, J., Evans, J.A., Tamstorf, R., 2022. Constructing nitsche's method for variational problems. arXiv:2203.02603.

[9] Brezzi, F., Marini, L.D., Süli, E., 2004. Discontinuous galerkin methods for first-order hyperbolic problems. Mathematical Models and Methods in Applied Sciences 14, 1893–1903. doi:10.1142/s0218202504003866.

[10] Bukač, M., Muha, B., Salgado, A.J., 2023. Analysis of a diffuse interface method for the stokes-darcy coupled problem. ESAIM: Mathematical Modelling and Numerical Analysis 57, 2623–2658. doi:10.1051/m2an/2023062.

[11] Burman, E., 2011. A penalty free non-symmetric nitsche type method for the weak imposition of boundary conditions. arXiv:1106.5612.

[12] Cavalheiro, A.C., 2008. Weighted sobolev spaces and degenerate elliptic equations. Boletim da Sociedade Paranaense de Matemática 26. doi:10.5269/bspm.v26i1-2.7415.

[13] Chadwick, A.F., Stewart, J.A., Enrique, R.A., Du, S., Thornton, K., 2018. Numerical modeling of localized corrosion using phase-field and smoothed boundary methods. Journal of The Electrochemical Society 165, C633–C646. doi:10.1149/2.0701810jes.

[14] Chen, Y., Lowengrub, J.S., 2014. Tumor growth in complex, evolving microenvironmental geometries: A diffuse domain approach. Journal of Theoretical Biology 361, 14–30. doi:10.1016/j.jtbi.2014.06.024.

[15] Dedner, A., Nolte, M., Klöfkorn, R., . Python bindings for the dune-fem module. doi:10.5281/zenodo.3706994.

[16] Franz, S., Roos, H.G., Gärtner, R., Voigt, A., 2012. A note on the convergence analysis of a diffuse-domain approach. Computational Methods in Applied Mathematics 12, 153–167. doi:10.2478/cmam-2012-0017.

[17] Freund, J., Stenberg, R., 1995. On weakly imposed boundary conditions for second order problems, in: Proceedings of the Ninth International Conference on Finite Elements in Fluids, pp. 327–336.

[18] Fries, T.P., Belytschko, T., 2010. The extended/generalized finite element method: An overview of the method and its applications. International Journal for Numerical Methods in Engineering 84, 253–304. doi:10.1002/nme.2914.

[19] Geuzaine, C., Remacle, J.F., 2009. Gmsh: A 3-d finite element mesh generator with built-in pre- and post-processing facilities. International Journal for Numerical Methods in Engineering 79, 1309–1331. doi:10.1002/nme.2579.

[20] Glowinski, R., Pan, T., Wells Jr., R.O., Zhou, X., 1996. Wavelet and finite element solutions for the neumann problem using fictitious domains. Journal of Computational Physics 126, 40–51. doi:10.1006/jcph.1996.0118.

[21] Griffith, B.E., Patankar, N.A., 2020. Immersed methods for fluid-structure interaction. Annual Review of Fluid Mechanics 52, 421–448. doi:10.1146/annurev-fluid-010719-060228.

[22] Guermond, J.L., Minev, P., Shen, J., 2006. An overview of projection methods for incompressible flows. Computer Methods in Applied Mechanics and Engineering 195, 6011–6045. doi:10.1016/j.cma.2005.10.010.

[23] Guermond, J.L., Quartapelle, L., 1998. On incremental projection methods, in: Research Notes in Mathematics Series, CRC Press. pp. 277–288.

[24] Guo, Z., Yu, F., Lin, P., Wise, S., Lowengrub, J., 2021. A diffuse domain method for two-phase flows with large density ratio in complex geometries. Journal of Fluid Mechanics 907. doi:10.1017/jfm.2020.790.

[25] John, V., 2002. Higher order finite element methods and multigrid solvers in a benchmark problem for the 3d navier-stokes equations. International Journal for Numerical Methods in Fluids 40, 775–798. doi:10.1002/fld.377.

[26] John, V., 2004. Reference values for drag and lift of a two-dimensional time-dependent flow around a cylinder. International Journal for Numerical Methods in Fluids 44, 777–788. doi:10.1002/fld.679.

[27] John, V., 2016. Finite Element Methods for Incompressible Flow Problems. Springer International Publishing.

[28] Juntunen, M., Stenberg, R., 2009. Nitsche's method for general boundary conditions. Mathematics of Computation 78, 1353–1374. doi:10.1090/s0025-5718-08-02183-2.

[29] Kilian, S., Turek, S., 2002. The Virtual Album of Fluid Motion. Springer Berlin, Heidelberg. URL: https://www.mathematik.tu-dortmund.de/~featflow/album/.

[30] Kockelkoren, J., Levine, H., Rappel, W.J., 2003. Computational approach for modeling intra- and extracellular dynamics. Physical Review E 68, 37–702. doi:10.1103/physreve.68.037702.

[31] Lervåg, K.Y., Lowengrub, J., 2015. Analysis of the diffuse-domain method for solving pdes in complex geometries. Communications in Mathematical Sciences 13, 1473–1500. doi:10.4310/CMS.2015.v13.n6.a6.

[32] LeVeque, R.J., Li, Z., 1994. The immersed interface method for elliptic equations with discontinuous coefficients and singular sources. SIAM Journal on Numerical Analysis 31, 1019–1044. doi:10.1137/0731054.

[33] Li, X., Lowengrub, J., Ratz, A., Voigt, A., 2009. Solving pdes in complex geometries: A diffuse domain approach. Communications in Mathematical Sciences 7, 81–107. doi:10.4310/cms.2009.v7.n1.a4.

[34] Loy, K.C., Bourgault, Y., 2017. On efficient high-order semi-implicit time-stepping schemes for unsteady incompressible navier-stokes equations. Computers & Fluids 148, 166–184. doi:10.1016/j.compfluid.2017.02.017.

[35] Monte, E.J., Lowman, J., Abukhdeir, N.M., 2022. A diffuse interface method for simulation-based screening of heat transfer processes with complex geometries. The Canadian Journal of Chemical Engineering 100, 3047–3062. doi:10.1002/cjce.24320.

[36] Nguyen, L., Stoter, S., Baum, T., Kirschke, J., Ruess, M., Yosibash, Z., Schillinger, D., 2017a. Phase-field boundary conditions for the voxel finite cell method: Surface-free stress analysis of ct-based bone structures. International Journal for Numerical Methods in Biomedical Engineering 33. doi:10.1002/cnm.2880.

[37] Nguyen, L.H., Stoter, S.K.F., Ruess, M., Sanchez Uribe, M.A., Schillinger, D., 2017b. The diffuse nitsche method: Dirichlet constraints on phase-field boundaries. International Journal for Numerical Methods in Engineering 113, 601–633. doi:10.1002/nme.5628.

[38] Parussini, L., Pediroda, V., 2009. Fictitious domain approach with hp-finite element approximation for incompressible fluid flow. Journal of Computational Physics 228, 3891–3910. doi:10.1016/j.jcp.2009.02.019.

[39] de Prenter, F., Verhoosel, C.V., van Brummelen, E.H., Larson, M.G., Badia, S., 2023. Stability and conditioning of immersed finite element methods: analysis and remedies. Archives of Computational Methods in Engineering 30, 3617–3656. doi:10.1007/s11831-023-09913-0.

[40] Quilez, I., . 2d distance functions. https://iquilezles.org/articles/distfunctions2d/.

[41] Ramière, I., Angot, P., Belliard, M., 2007. A general fictitious domain method with immersed jumps and multilevel nested structured meshes. Journal of Computational Physics 225, 1347–1387. doi:10.1016/j.jcp.2007.01.026.

[42] Rätz, A., 2016. Diffuse-interface approximations of osmosis free boundary problems. SIAM Journal on Applied Mathematics 76, 910–929. doi:10.1137/15m1025001.

[43] Rätz, A., Voigt, A., 2006. Pde's on surfaces - a diffuse interface approach. Communications in Mathematical Sciences 4, 575–590. doi:10.4310/cms.2006.v4.n3.a5.

[44] Sander, O., 2020. DUNE - The Distributed and Unified Numerics Environment. Springer International Publishing.

[45] Schäfer, M., Turek, S., Durst, F., Krause, E., Rannacher, R., 1996. Benchmark Computations of Laminar Flow Around a Cylinder. Vieweg+Teubner Verlag. pp. 547–566. doi:10.1007/978-3-322-89849-4_39.

[46] Stoter, S.K.F., ten Eikelder, M.F.P., de Prenter, F., Akkerman, I., van Brummelen, E.H., Verhoosel, C.V., Schillinger, D., 2021. Nitsche's method as a variational multiscale formulation and a resulting boundary layer fine-scale model. Computer Methods in Applied Mechanics and Engineering 382, 113878. doi:10.1016/j.cma.2021.113878.

[47] Sutton, O.J., 2018. Long-time l∞(l2) a posteriori error estimates for fully discrete parabolic problems. IMA Journal of Numerical Analysis 40, 498–529. doi:10.1093/imanum/dry078.

[48] Taylor, G.I., Green, A.E., 1937. Mechanism of the production of small eddies from large ones. Proceedings of the Royal Society of London. Series A, Mathematical and Physical Sciences 158, 499–521. doi:10.1098/rspa.1937.0036.

[49] Teigen, K.E., Li, X., Lowengrub, J., Wang, F., Voigt, A., 2009. A diffuse-interface approach for modelling transport, diffusion and adsorption/desorption of material quantities on a deformable interface. Communications in Mathematical Sciences 7, 1009–1037. doi:10.4310/cms.2009.v7.n4.a10, arXiv:PMC3046400.

[50] Termuhlen, R., Fitzmaurice, K., Yu, H.C., 2022. Smoothed boundary method for simulating incompressible flow in complex geometries. Computer Methods in Applied Mechanics and Engineering 399. doi:10.1016/j.cma.2022.115312.

[51] Vos, P.E.J., van Loon, R., Sherwin, S.J., 2008. A comparison of fictitious domain methods appropriate for spectral/hp element discretisations. Computer Method , 2275–2289doi:10.1016/j.cma.2007.11.023.

[52] Yu, F., Guo, Z., Lowengrub, J., 2020. Higher-order accurate diffuse-domain methods for partial differential equations with dirichlet boundary conditions in complex, evolving geometries. Journal of Computational Physics 406, 109–174. doi:10.1016/j.jcp.2019.109174.

[53] Yu, H.C., Chen, H.Y., Thornton, K., 2009. Smoothed boundary method for solving partial differential equations with general boundary conditions on complex boundaries. arXiv:0912.1288.

[54] Yu, H.C., Chen, H.Y., Thornton, K., 2012. Extended smoothed boundary method for solving partial differential equations with general boundary conditions on complex boundaries. Modelling and Simulation in Materials Science and Engineering 20, 075008. doi:10.1088/0965-0393/20/7/075008.

Appendix A. Advection-Diffusion Numerical Results

Here we show the results for all approaches tested for the problems in Section 6.1. Figure A.12 shows the legend for the approaches, the order of basis functions, and the error measurement; this matches the earlier plots.

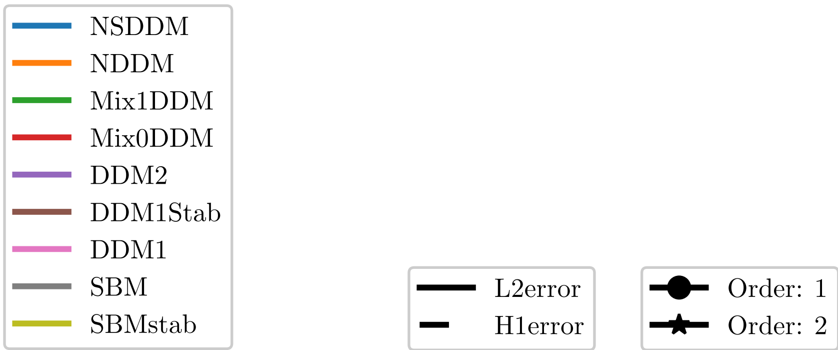

Figure A.12: Legends for all pots in section Appendix A.

Appendix A.1. Diffusion Dominated

Figures A.13A.14A.15A.16 show the results for the diffusion dominated problem. It is clear that Mix0DDM is performing better than Mix1DDM, and NSDDM better than NDDM. Importantly, they are showing lower errors and better convergence than the traditional approaches of DDM1 and SBM.

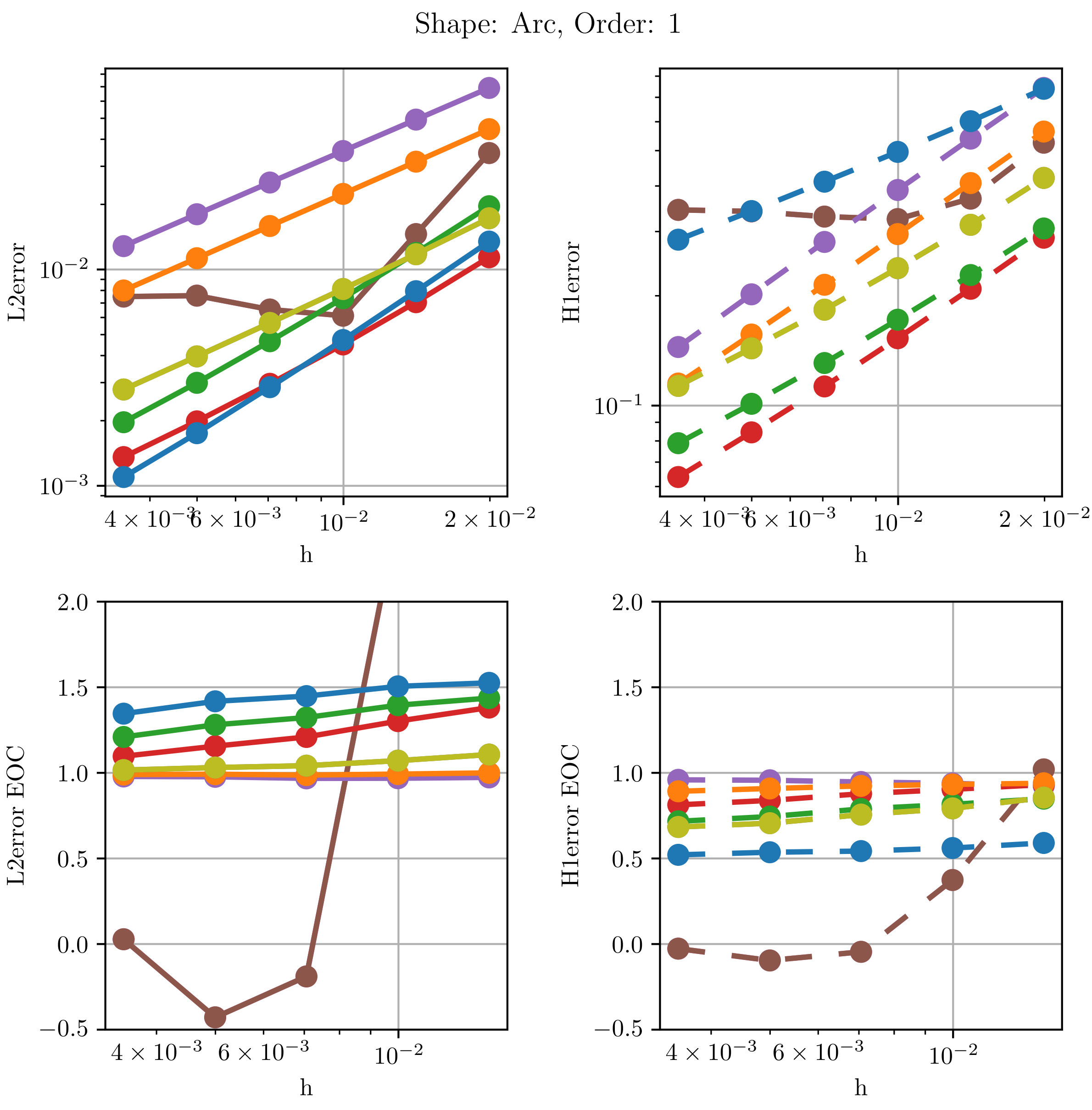

Figure A.13: Diffusion Dominated problem error plot for Arc domain with linear elements.

Shape: Arc, Order: 2

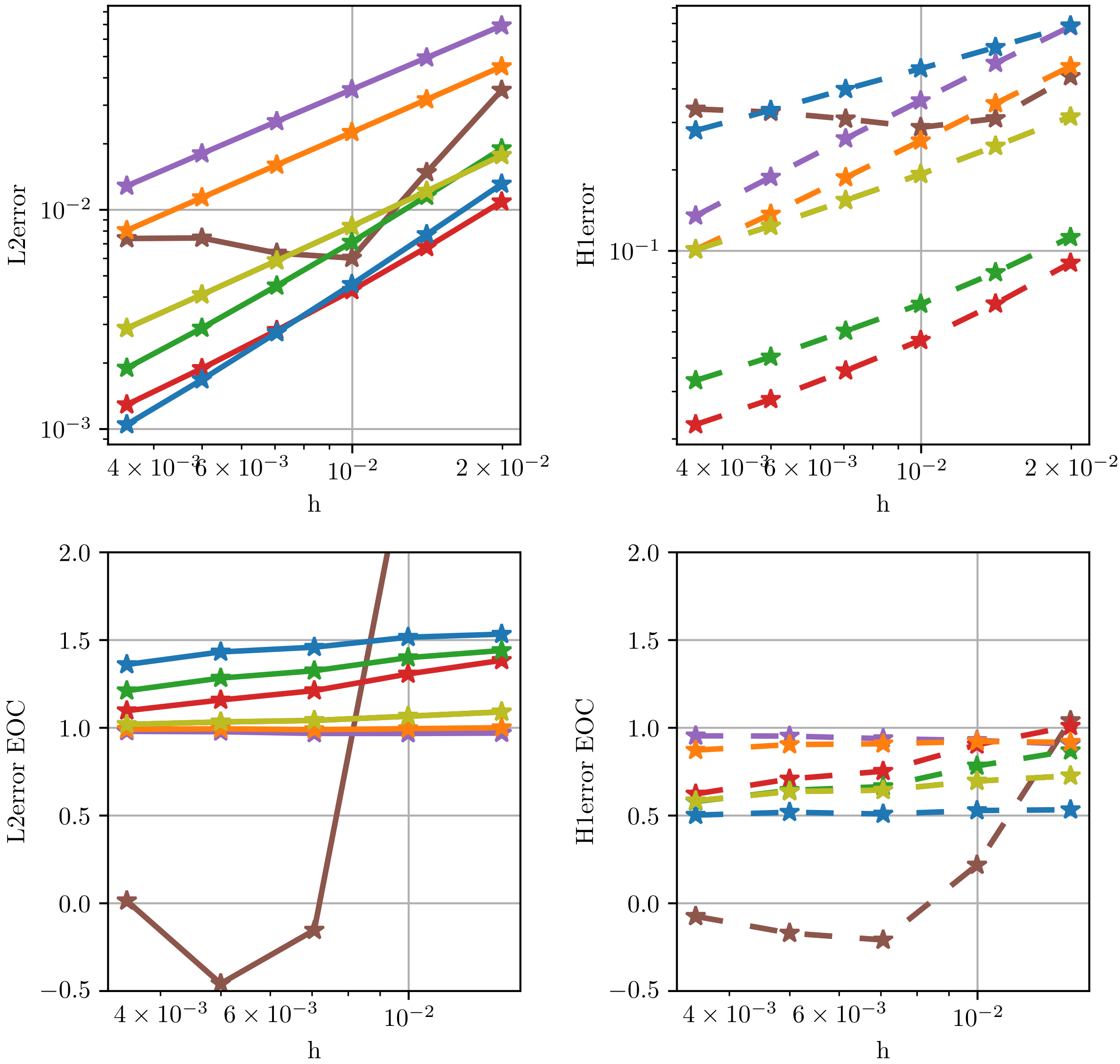

Figure A.14: Diffusion Dominated problem error plot for Arc domain with quadratic elements.

Shape: Arc Inv, Order: 1

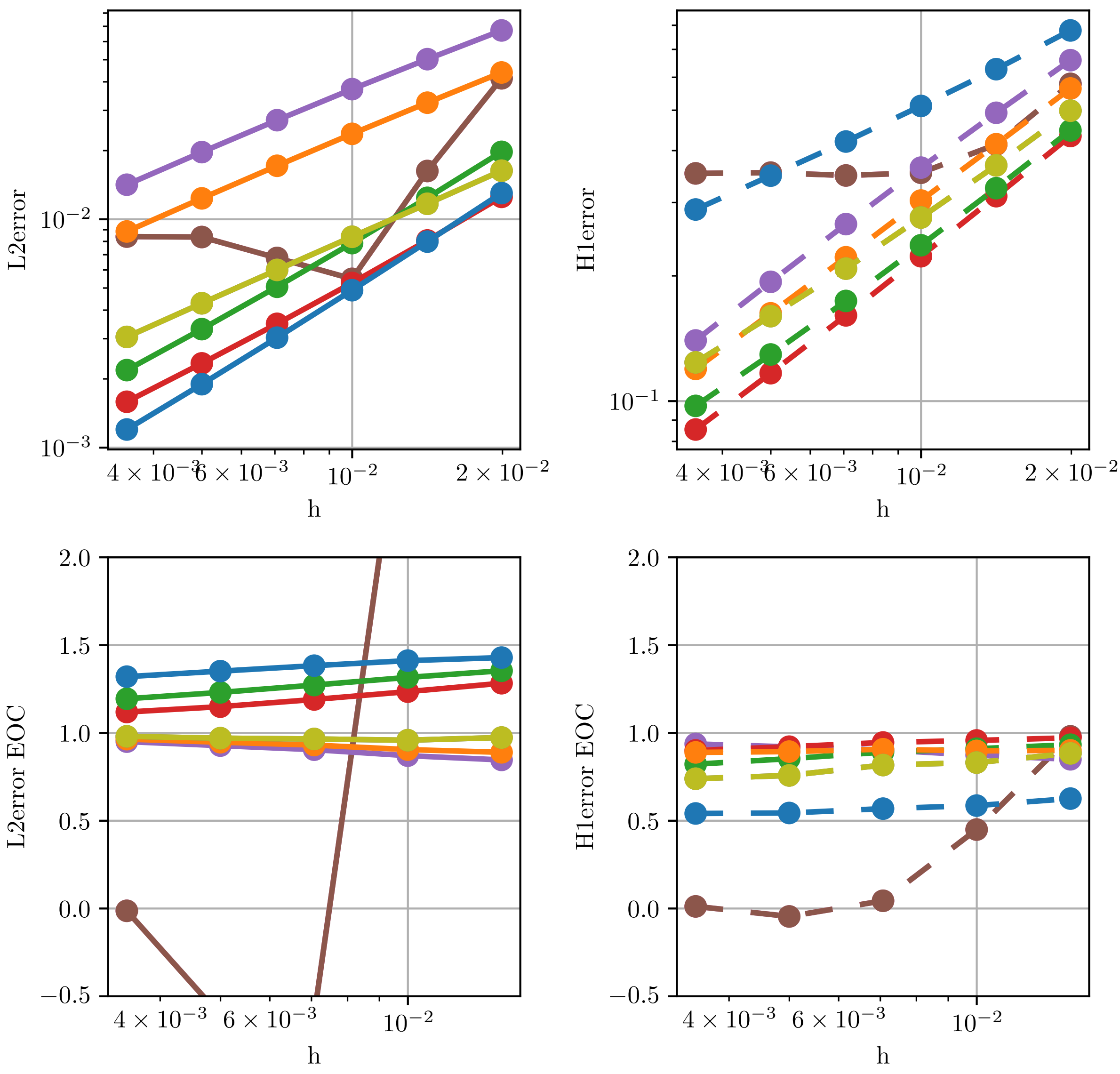

Figure A.15: Diffusion Dominated problem error plot for Inverted Arc domain with linear elements.

Shape: Arc Inv, Order: 2

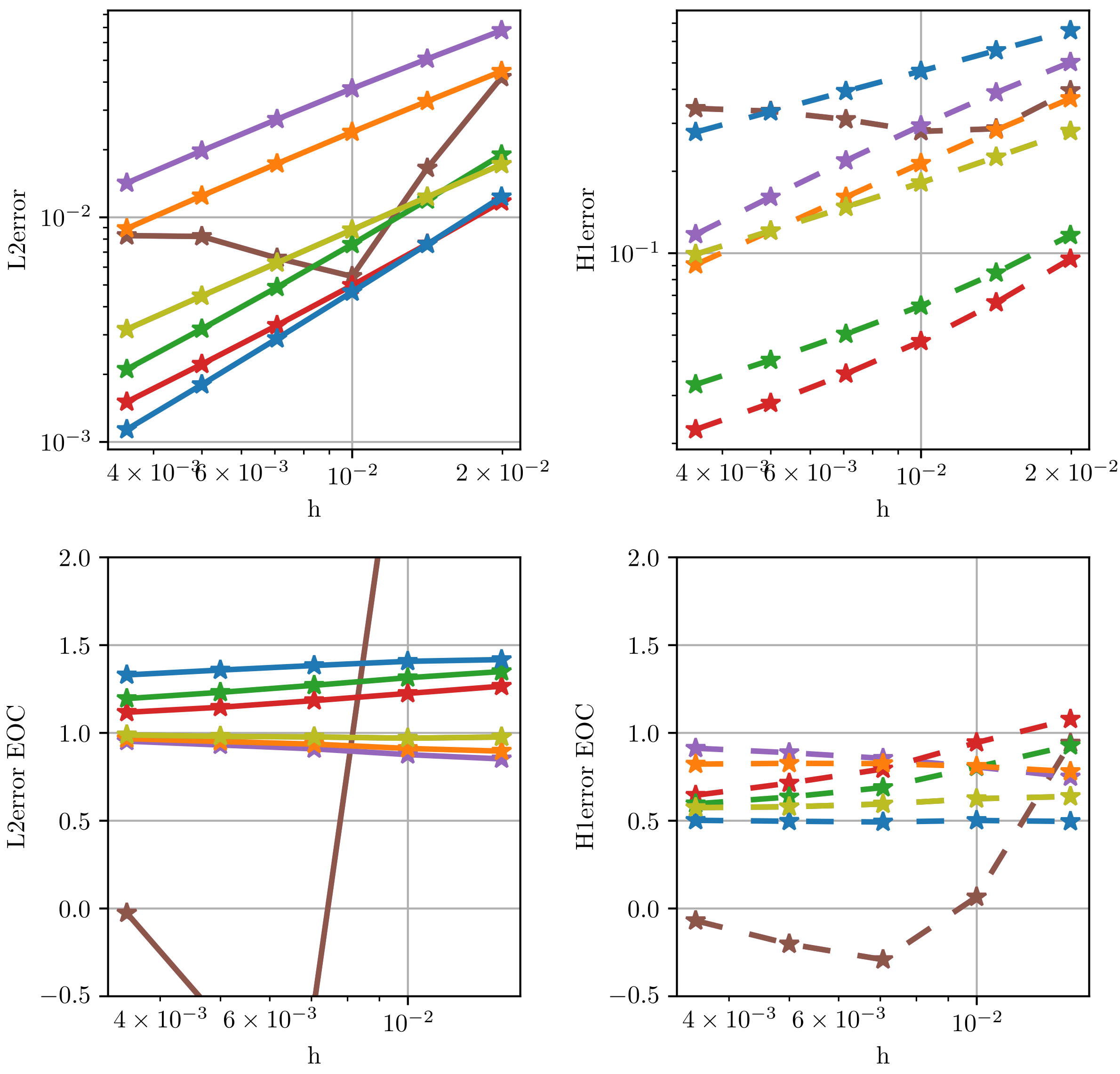

Figure A.16: Diffusion Dominated problem error plot for Inverted Arc domain with quadratic elements.

Appendix A.2. Advection Dominated

Figures A.17A.18A.19A.20 show the results for the advection dominated problem, which are similar to the above diffusion dominated problem. We can see the impact of the stabilised terms on DDM1 and SBM, which show stabilised SBM error is a smaller magnitude but slower convergence.

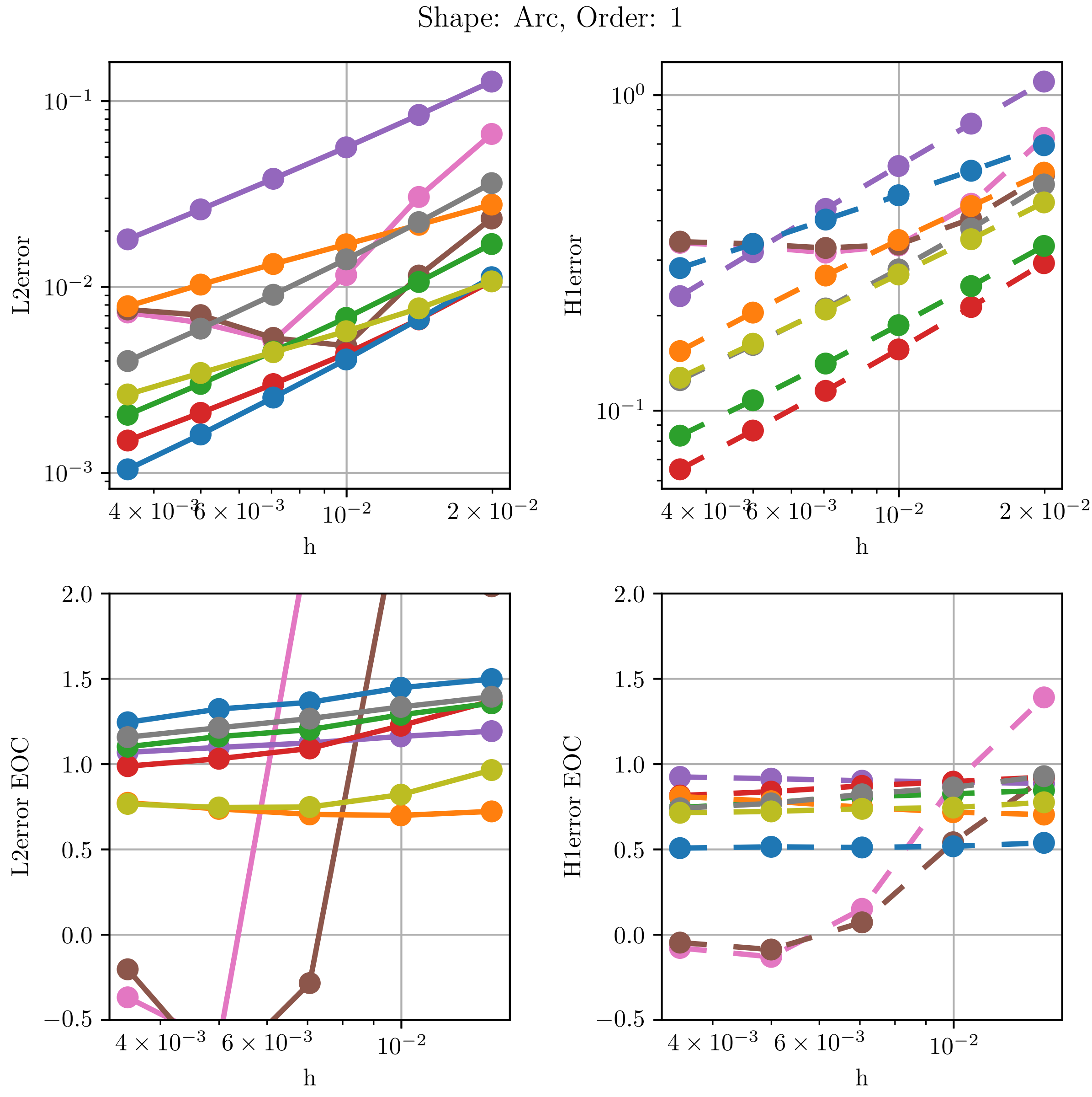

Figure A.17: Advection Dominated problem error plot for Arc domain with linear elements.

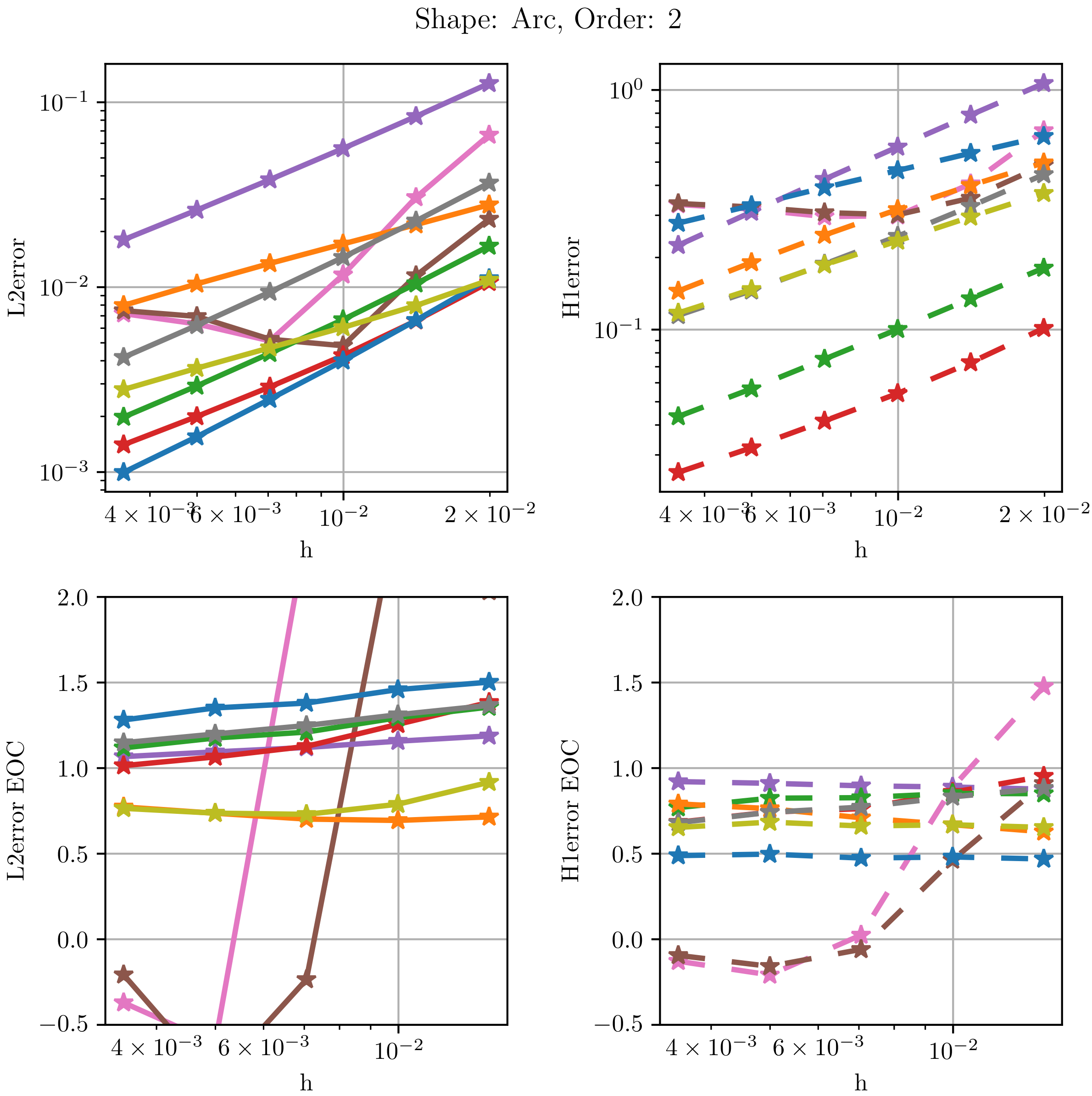

Figure A.18: Advection Dominated problem error plot for Arc domain with quadratic elements.

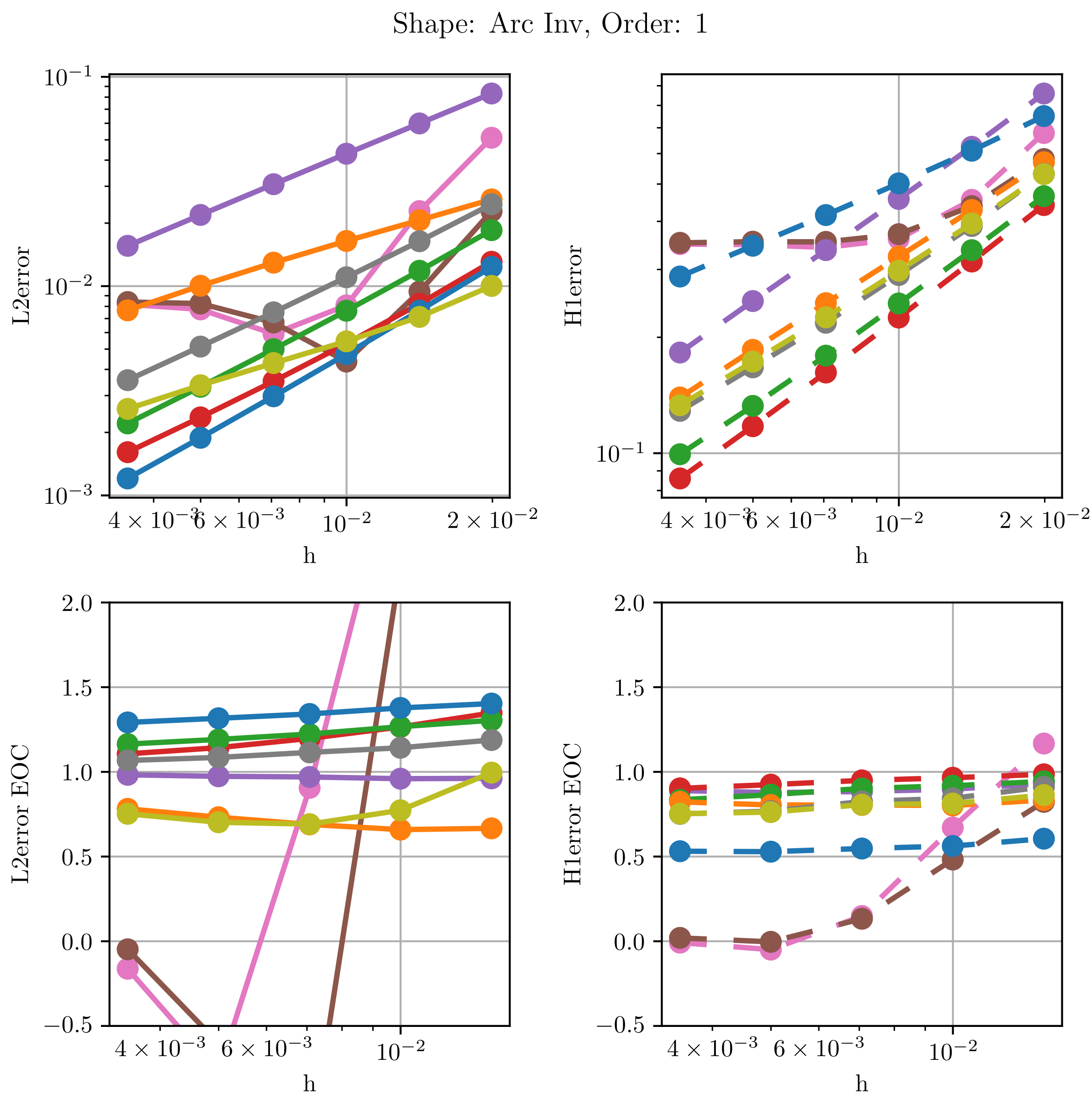

Figure A.19: Advection Dominated problem error plot for Inverted Arc domain with linear elements.

Shape: Arc Inv, Order: 2

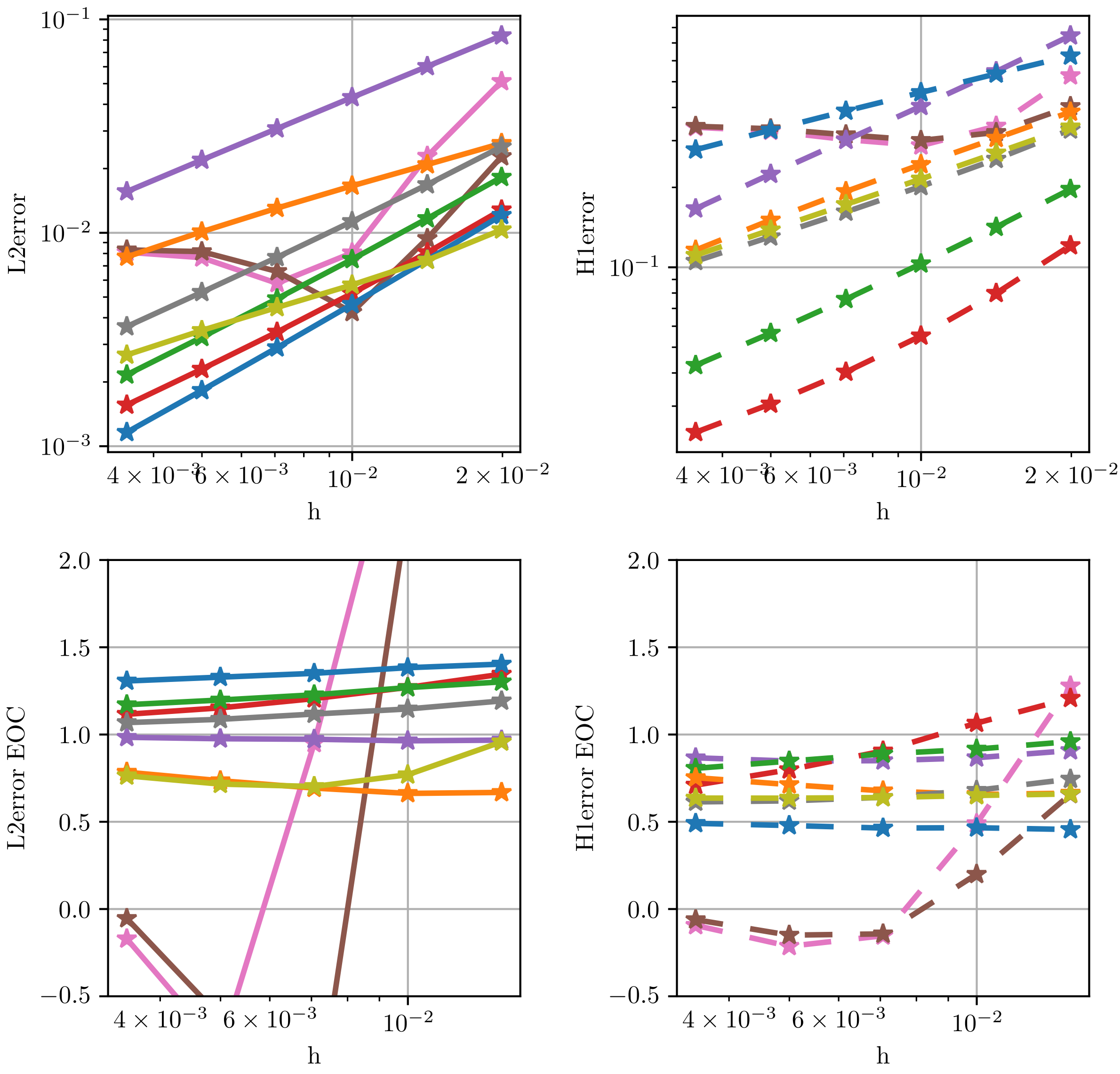

Figure A.20: Advection Dominated problem error plot for Inverted Arc domain with quadratic elements.